Research Programme of the Research Fund for Coal and Steel

Steel RTD

Project carried out with a financial grant of the
Research Programme of the Research Fund for Coal and Steel

Robustness of car parks against localised fire

Grant Agreement Number RFSR-CT-2008-00036

Deliverable IV: Development of FEM model for car parks under localised fire

March 2012

Authors: Cheng Fang (ICST)

Bassam Izzuddin (ICST)

Ahmed Elghazouli (ICST)

David Nethercot (ICST)

Ludivine Comeliau (ULGG)

Jean-Pierre Jaspart (ULGG)

Jean-François Demonceau (ULGG)

Cécile Haremza (FCTUCOIMBRA)

Aldina Santiago (FCTUCOIMBRA)

Luís Simões da Silva (FCTUCOIMBRA)

Renata Obiala (ARCELORPROFIL)

Bin Zhao (CTICM)

Dhionis Dhima (CSTB)

Frédéric Gens (GREISCH)

Vincent de Ville (GREISCH)

Table of contents

Annex A – Benchmark studies of floor slab

Annex B – FEM simulation of sub-frame

Annex C – Multi-level modelling strategy and verification

I. Introduction

The main task of WP3 is to integrate the knowledge acquired on elements in WP2 into a structural model enabling prediction of the integrated structural response under localised fire. Two main objectives of WP3 are identified:

- the development of FEM simulations of the whole structure subjected to localised fire;
- practical behavioural models for the whole structure for design practice.

This deliverable summarises the outcomes related to three aspects: FEM simulation of composite floor slabs, FEM simulation of sub-frames, and FEM multi-level system modelling. The behavioural models predicting the response of car parks by means of "practice-oriented" approaches will be further presented in Deliverable V. Under the framework of this deliverable, a slab benchmark study conducted by Imperial College London (IC) and the University of Liège (ULg) is reported first. Subsequently, a detailed finite element model is presented by the University of Coimbra (UC) to study the behaviour of a composite steel-concrete sub-frame under localised fire, where the commercial finite element package ABAQUS, 2011 is used. Finally, a multi-level structural modelling approach, which can satisfy various design requirements, is developed by IC. The rationale behind the proposed modelling reducing procedure is justified.

II. FEM simulation of composite floor and slab benchmark study

In order to study both the ambient and elevated temperature properties of composite slabs, and to validate the numerical tools, FE models of slabs were established and a benchmark study was conducted by IC and ULg with two finite element software packages, ADAPTIC (Izzuddin, 1991) and SAFIR (Franssen, 2005). The parameters considered in the benchmark study include:

- slab profile
- material nonlinearity
- boundary conditions
- contribution from secondary beams

The studied slabs are 16m×10m isolated composite slabs. The basic outlines of the slab models (both uniform slab and ribbed slab) are illustrated in Figure 1, and the corresponding dimensions are listed in Table 1, where a is the slab length, b is the slab width, t is the thickness of steel deck, d is the depth for uniform slab, s is the distance from the top of the slab to the location of reinforcement. In addition, for the slab with ribbed profile, d_1 is the thickness of the cover, d_2 is the thickness of the rib, w_1 is the width of the rib bottom, and w_2 is the width of the rib top. For both of the uniform thickness slab (reference case) and the ribbed slab, the location of reinforcement mesh is 50mm below the top face of the slab. It is assumed that the slab is simply supported, though the planar displacements at the supports may either be restrained or unrestrained. The steel deck is assumed to be unidirectional, acting only along the rib direction while no action is considered along the transverse direction.

Table 1. Values of slab dimensions

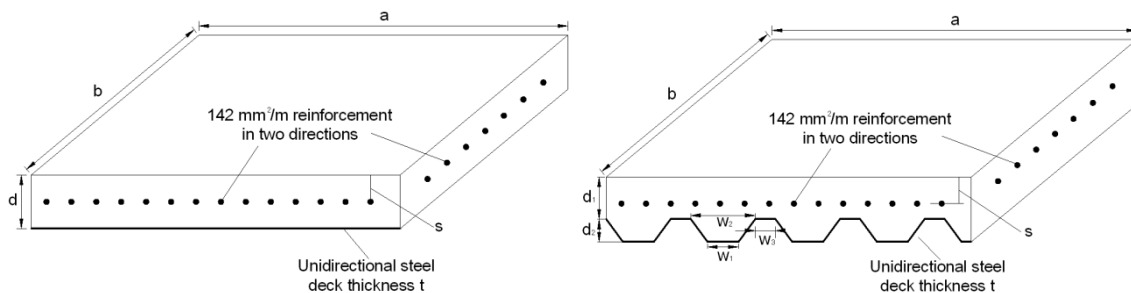| Dimensions(mm)	a	b	d	d_1	d_2	w_1	w_2	w_3	t	s
Value	16000	10000	100	70	60	272	376	224	0.9	50

Figure 1. Geometric properties of slab

For the study of the ambient cases, an increasing uniformly distributed load is applied on the slab until very large deformation. With regard to the fire situation, a constant uniform distributed load of 5kN/m^2 is applied on the slab, and a linear temperature gradient is assumed over the depth. The temperature of the bottom face of the slab linearly increases from the ambient temperature (0ºC) to 900ºC, while the temperature of the top face of the slab remains under the ambient condition. The temperature distribution along the length/width of the slab is assumed to be uniform. The thermal characteristics for steel and concrete are based on EN1993-1-2, 2005 and EN1994-1-2, 2005, respectively.

Since different FE software packages were employed, the slab modelling strategies slightly vary. Details of the FE modelling methods as well as the comparisons of the results predicted by the two software packages are reported in **Annex A**.

III.   FEM simulation of sub-frame

A finite element model, as shown in Figure 2, was developed in UC to study the behaviour of a composite steel-concrete sub-frame. The commercial general finite element package ABAQUS (2011) was used to model the composite steel-concrete beam-to-column frame extracted from the designed open car park building in accordance with WP5. The main objective is to study the detailed behaviour of the composite sub-frame as accurately as possible. Materials for steel members and connection components are established by steel tensile coupon tests, whereas the concrete behaviour is defined according to Eurocode 2 part 1.1 (EN 1992-1-1:2004). Details of the 3D FE model are provided in **Annex B**.
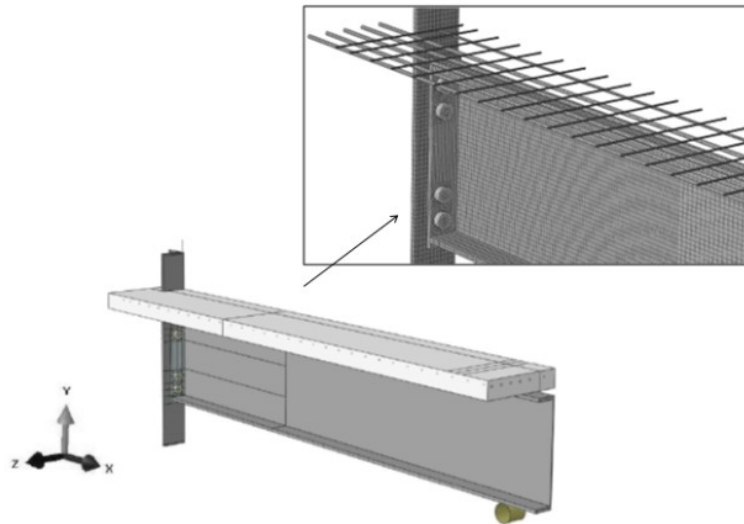

Figure 2. 3D FE model of sub-frame in Abaqus

IV.   Multi-level structural modelling

Three modelling levels were proposed by IC, as shown in Figure 3. At Level A, consideration is given to a whole system of an influenced sub-structure with appropriate boundary conditions to represent the surrounding cool structures. The interactions among the heated column, the fire affected floor and the upper ambient floors are fully considered. Provided that the upper ambient floor systems have identical structural type and applied loading, the assessment model can be simplified to Level B, where a reduced model consisting of a fire affected floor-column system and a spring representing the upper ambient floor systems are considered. At this level, the two systems (i.e. fire and ambient) are investigated separately. The derived characteristics of the ambient floors can be applied into the nonlinear spring. At Level C, planar effects within the floor slab are ignored, and grillage models with composite beams are considered instead.
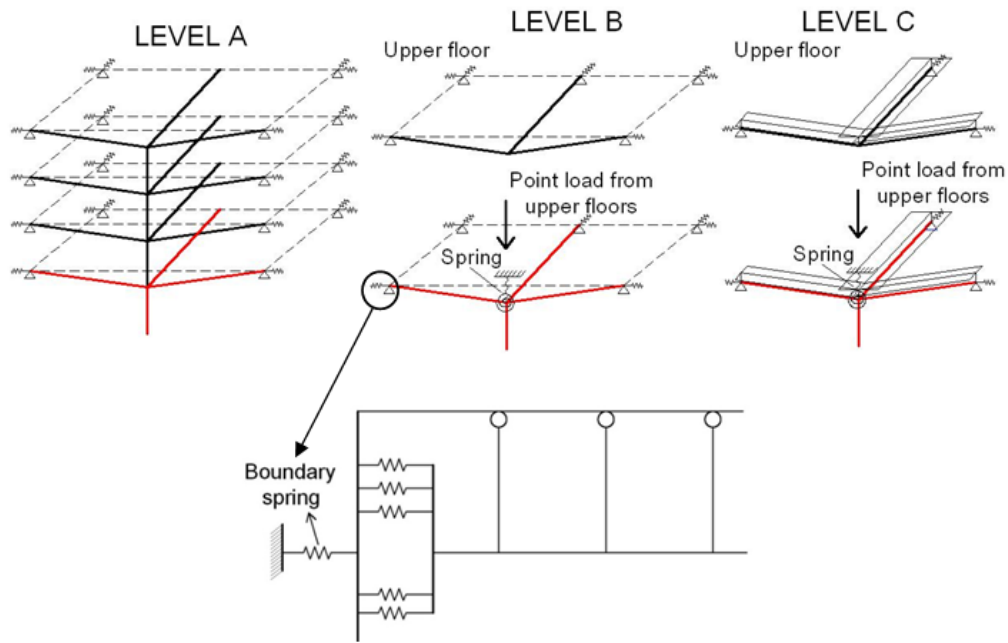
Figure 3. Illustrative descriptions of the three proposed modelling levels

In order to verify the accuracy of the proposed model reduction procedure, a four-storey steel-framed composite structure is established in ADAPTIC, as shown in Figure 4(a). Joint details are ignored in the model, and beams and columns are assumed to be rigidly connected. It is assumed that the internal column at the ground floor experiences a uniform increase in temperature, and this temperature reduces linearly from the column top to room temperature 3m away from the column within the connected steel beams. The slab is considered as fully protected and remains under ambient conditions throughout the heating procedure. This model is then reduced to a level C model comprising the fire floor system and an additional spring, as shown in Figure 4(b). In ADAPTIC, the spring is modelled using an element that is capable of simulating the force-displacement relationships with multi-linear approximations. The loads exerted onto the reduced model include a 5kN/m^2 UDL, a point load from the upper three ambient floors and the subsequent thermal load. Details of the verification of the model reducing procedure are elaborated in **Annex C**.
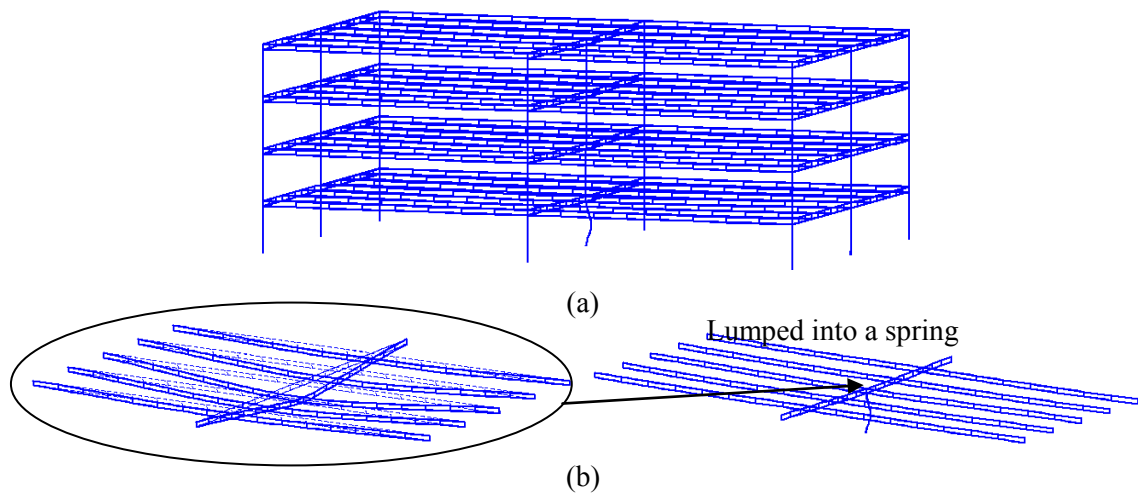

(a)

(b)

Figure 4. ADAPTIC model with internal column under fire: (a) 4-storey model, (b) reduced system model

5

V. Conclusions

This deliverable presents the FEM modelling method in an incremental manner, from floor slab model to sub-frame model, and finally towards the multi-level system modelling strategy.

The aim of slab benchmark study is to ensure that the results of slab analysis from the two nonlinear finite element tools are comparable, so as to guarantee sufficient accuracy in modelling the ambient and elevated temperature response of floor systems. A close comparison is generally found between ADAPTIC and SAFIR, which indicates that the slab response can be predicted with sufficient accuracy using either of the two programs. Regarding the sub-frame, the detailed ABAQUS model is shown to be capable of simulating the tested sub-frame (WP2) with sound accuracy. Finally, the proposed model reduction approach is shown to simplify the complex multi-storey structural model into the reduced single-storey system model with negligible loss of accuracy, provided that the response of upper ambient floors is appropriately predicted. Therefore, efficient reduced system models can be used for evaluations of structural behaviour or assessments of structural robustness of buildings subject to localised fires in later studies.

VI.   References

ABAQUS (2011). Analysis User's manual, v6.11, Dassault Systems Simulia Corp., Providence, USA.

CEB (1990). "CEB-FIP – Model Code", Comité euro-international du béton, Design code, Thomas Telford Services Ltd.

EN 1992-1-1:2004, "Eurocode 2: Design of concrete structures - Part 1-1: General rules and rules for buildings", European committee for standardization, December 2004.

Izzuddin B.A. (1991). "Nonlinear Dynamic Analysis of Framed Structures", PhD Thesis, Imperial College, University of London.

SAFIR. Franssen J. M. (2005). "A Thermal/Structural Program Modelling Structures under Fire", Engineering Journal, AISC, 42:3, 143-158, http://hdl.handle.net/2268/2928.

ANNEX A

ROBUSTFIRE REPORT

Benchmark study of floor slab

Imperial College London

Cheng Fang

Bassam Izzuddin

Ahmed Elghazouli

David Nethercot

Université de Liège

T Gernay

J-F Demonceau

J-M Franssen

Contents

I Introduction

Concrete/composite slabs can play a significant role in the robustness of a composite structural system. Recent experimental research, including the Cardington fire testing programme, has shown that the slab membrane action can effectively carry extensive loads in double span when an internal column and the adjacent members are affected. In order to study both the ambient and elevated temperature properties of composite slabs and validate the capability of numerical tools in predicting the related response, a benchmark study is proposed, where the slab profile, material nonlinearity, boundary conditions and the contribution of secondary beams are considered.

Two finite element software packages (ADAPTIC and SAFIR) are employed in this study. In ADAPTIC (Izzuddin,1991), a new shell element was developed by Izzuddin *et al.* (2004) for the realistic modelling of composite and reinforced concrete floor slabs (considering the geometric orthotropy of ribbed slab) subject to extreme loading conditions. Extensive validation of this slab model against experimental results on flat and ribbed reinforced concrete/composite floor slabs has already been undertaken (Elghazouli &Izzuddin, 2004). Here, further verification of this model will be conducted.

SAFIR (Franssen, 2005) is a special-purpose computer program for the analysis of structures under ambient and elevated temperature conditions. This program can be used to study the behaviour of one, two and three-dimensional structures. This program was developed at Liège University, Belgium, and is today viewed as the second generation of structural fire codes developed in Liège, the first generation being another computer program called 'Computer Engineering of the Fire design of Composite and Steel Structures (CEFICOSS)'. As a finite element program, SAFIR accommodates various elements for different idealization, calculation procedures and various material models for incorporating stress-strain behaviour. The elements include the 2-D SOLID elements, 3-D SOLID elements, BEAM elements, SHELL elements and TRUSS elements. The stress-strain material laws are generally linear-elliptic for steel and non-linear for concrete.

II Model description

II.1 General

The studied slab is a 16m×10m isolated composite slab without the adjacent sub-structures. The basic outlines of the slab models (both uniform slab and ribbed slab) are illustrated in Figure 1 and the corresponding dimensions are listed in Table1, where a is the slab length, b is the slab width, t is the thickness of steel deck, d is the depth for uniform slab, s is the distance from the location of reinforcement to the top. In addition, for the slab with ribbed profile, d_1 is the thickness of the cover, d_2 is the thickness of the rib, w_1 is the width of the rib bottom, and w_2 is the width of the rib top.

For both the uniform thickness slab (reference case) and the ribbed slab, the locations of reinforcement mesh are 50mm below the top face of the slab. It is assumed that the slab is simply supported, though the planar support displacements may either be restrained or unrestrained. The steel deck is assumed to be unidirectional, which means that it only acts along the ribs direction while no action is considered along the cross direction. Therefore, the equivalent area for steel deck can be modelled as $900mm^2/m$ and $982mm^2/m$ for uniform and ribbed slabs respectively, and $0mm^2/m$ along the cross direction for both cases.

Table1: Values of slab dimensions

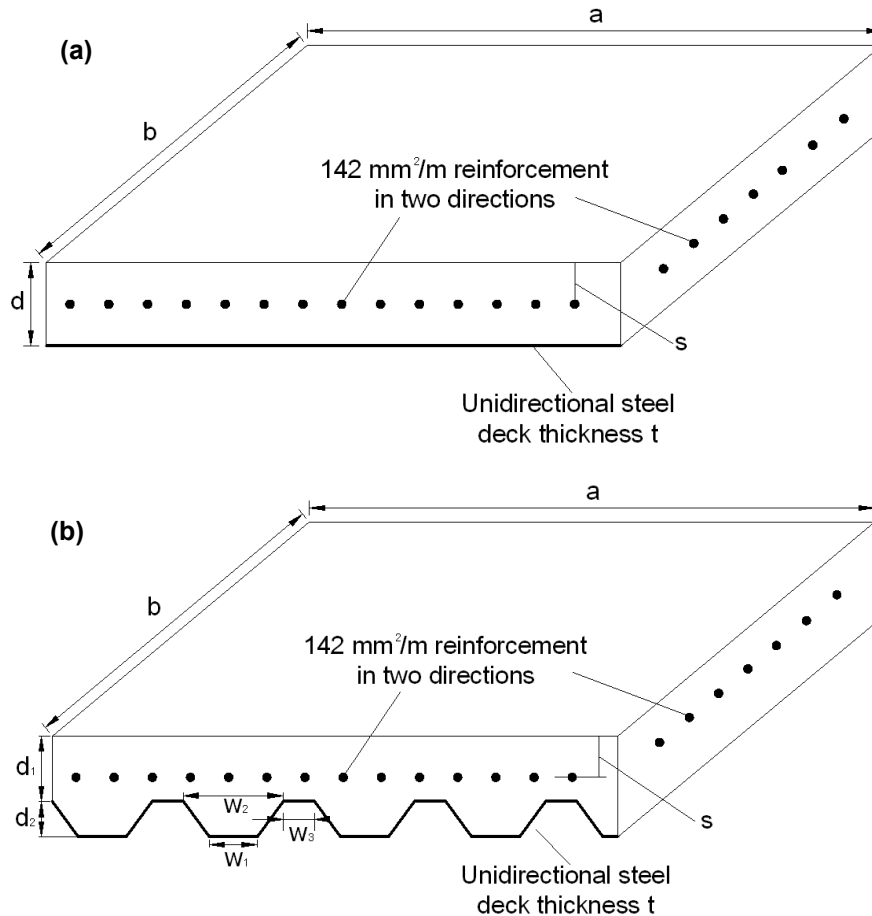| Dimensions(mm)	a	b	d	d_1	d_2	w_1	w_2	w_3	t	s
Value	16000	10000	100	70	60	272	376	224	0.9	50

Fig. 1 Geometric configuration of slab, a) uniform slab, b) ribbed slab

An increasing uniformly distributed load is applied on the slab for the study of the ambient cases. With regard to the fire situation, a constant uniform distributed load of $5kN/m^2$ is applied onto the slab, and a linear temperature gradient is assumed over the depth. In ADAPTIC, The temperature of the bottom face of the slab linearly increases from ambient temperature (0^oC) to 900^oC, while the temperature of the top face of the slab remains at ambient temperature. The temperature distribution along

the length/width of the slab is assumed to be uniform. The thermal characteristics for steel and concrete are based on EN1993-1-2 (2005) and EN1994-1-2 (2005), respectively. In SAFIR, the same temperature distribution as ADAPTIC is assumed for the uniform slab. The ribbed slab is modelled by shell elements of 70 mm height associated with concrete rebars of 30,000 mm²/m in the rib direction in SAFIR. The concrete rebars are positioned at distance 98.4 mm from the top of the slab. The temperature of the bottom face of the slab (70 mm from the top) linearly increases from the room temperature (20°C) to 700°C, the temperature of the concrete rebars increases from the room temperature to 886°C (assumed uniform in all the rebars modelling the rib), and the temperature of the steel deck increases from the room temperature to 900°C. The temperature gradients in ADAPTIC and SAFIR for the ribbed and uniform slabs at the slab bottom temperature of 900°C are illustrated in Figures 2 and 3, respectively.
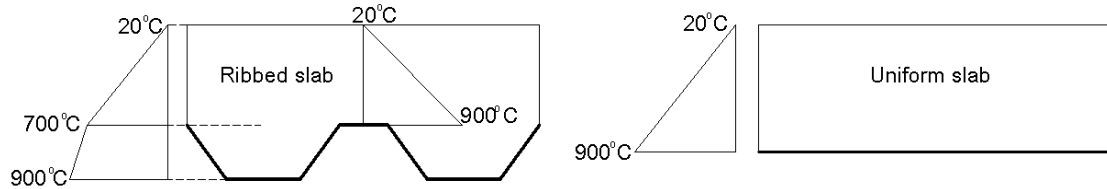

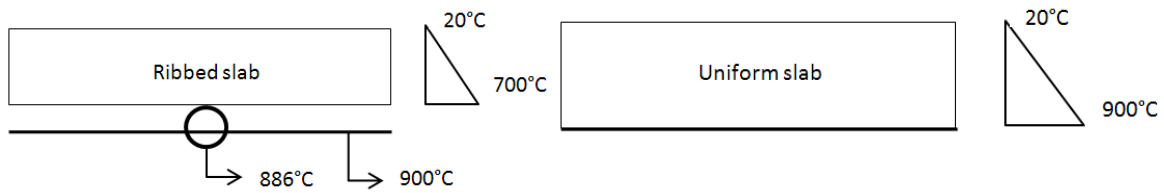Fig. 2 Illustration of temperature gradients of slabs in ADAPTIC

Fig. 3 Illustration of temperature gradients of slabs in SAFIR

II.2 Material modelling

Under the ambient temperature conditions, the same linear-elliptic material model is used for steel (EN1993-1-2, 2005) in both ADAPTIC and SAFIR, and the stress-strain diagram enters into a descending branch at a strain of 15%. For concrete, an advanced nonlinear concrete model, which accounts for the combined effects of compressive nonlinearity, tensile cracking opening and closure, and temperature, is employed in ADAPTIC. Details of this concrete model can be found elsewhere (Izzuddin et al., 2004). The basic ambient properties of concrete and steel in ADAPTIC are listed in Tables 2 and 3.

In SAFIR, since the Young's modulus for concrete is calculated from the compressive strength as $E(T) = \dfrac{3.f_c}{2.\varepsilon_{c1,\theta,EC2}(T)}$ which is a fixed value; the compressive strain ε_{c1} will be slightly different from ADAPTIC when the same value of Young's modulus E is used. The comparison of concrete stress-strain relationships in ADAPTIC and SAFIR is shown in Figure 4.
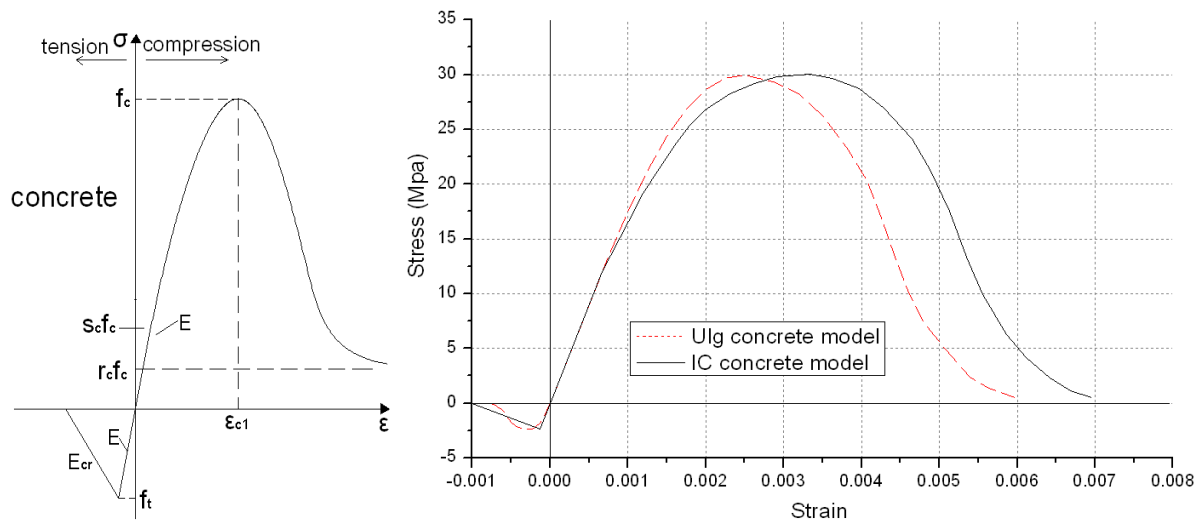
Fig. 4 Stress-strain relationships for concrete in ADAPTIC and SAFIR

Table 2: Ambient properties for steel in both ADAPTIC and SAFIR

Properties	Steel deck	Reinforcement
Young's modulus E (N/mm^2)	2.1×10^5	2.1×10^5
Yield strength f_y (N/mm^2)	3.0×10^2	6.0×10^2

Table 3: Ambient properties for concrete in ADAPTIC

Young's modulus E (N/mm^2)	1.8×10^4
Possion's ratio	0.2
Tensile strength f_t (N/mm^2)	2.36
Compressive strength f_c (N/mm^2)	30
Compressive strain ε_{c1}	0.0033
Tensile softening slope E_{cr} (N/mm^2)	2716
Normalised initial compressive strength s_c	0.4
Normalised residual compressive strength r_c	0.0
Factor for biaxial compressive interaction b_c	0.6
Elastic shear retention factor β_s	0.5
Factor scaling direct tensile stresses for shear Φ_s	0.5
Normalised shear softening relative to direct tensile softening γ_s	0.0

Table 4: Ambient properties for concrete in SAFIR

Young's modulus E (N/mm^2)	1.8×10^4 (calculated from f_c)
Poisson's ratio	0.2
Tensile strength ft (N/mm^2)	2.36
Compressive strength fc (N/mm^2)	30
Compressive strain ε_{c1}	0.0025
Normalised residual compressive strength r_c	0.0

With respect to the elevated temperature conditions, the key temperature-dependent material property degradations of steel and concrete in both ADAPTIC and SAFIR are according to EN1993-1-2 (2005) and EN1994-1-2 (2005), respectively. The same thermal expansion coefficients for steel and concrete are employed for ADAPTIC and SAFIR, as illustrated in Figures 5 and 6, where the curve for normal weight concrete (NC) is employed for the thermal expansion property of the concrete.
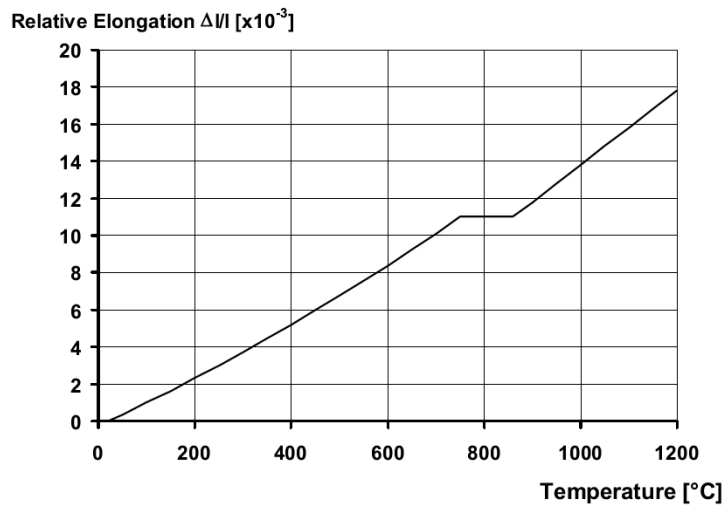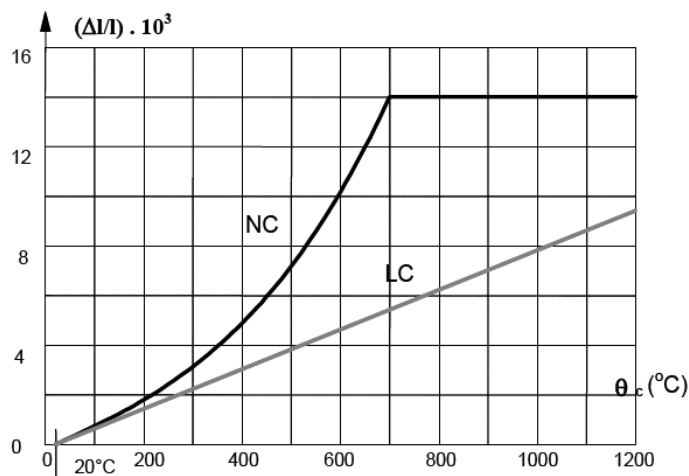

Fig. 5 Thermal strain for steel (EN1993-1-2, 2005)

Fig. 6 Thermal strain for concrete, curve NC (EN1994-1-2, 2005)

II.3 Case description

Five cases are considered in this study: 1) reference model, 2) ribbed slab model, 3) linear concrete model, 4) model without planar restraints, and 5) model with secondary beams. Ambient and fire analyses are applied with all models. The details of these models are discussed hereafter.

II.3.1 Reference case (model 1)

The reference case is considered as the slab with the following parameters:

- The slab is modelled as a uniform slab without the rib, and the value of $d=d_1+d_2/2=100$mm is assumed for the thickness of the reference slab.
- The slab is laterally restrained (in plane) and vertically supported along the four edges, while it is free to rotate at its boundaries.
- A full nonlinear response is assumed for concrete and steel.
- The secondary beams are not included.

The configuration of the reference model in ADAPTIC is shown in Figure 7
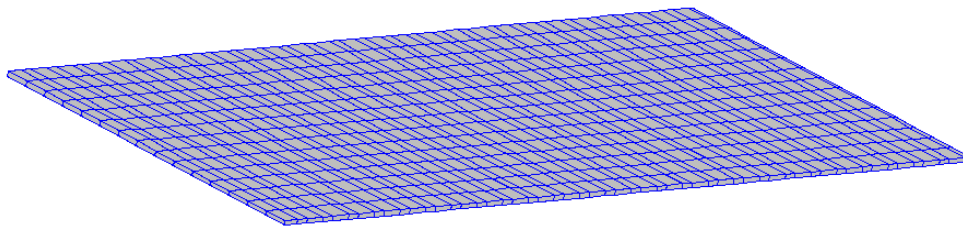

Fig. 7 Reference model in ADAPTIC

In SAFIR, the steel deck is modelled as an additional reinforcement mesh of 900 mm^2/m in the rib direction and 0 mm^2/m in the cross direction, positioned at the bottom of the slab. When modelling, the symmetry was taken into account and only a quarter of the slab was modelled for the study. Consequently, the appropriate boundary conditions were imposed on the edges of symmetry, which are:

- No in plane displacement perpendicular to the considered edge.
- No rotation with respect to the axe of the considered edge.
- No rotation with respect to the axe perpendicular to the plane of the slab.

II.3.2 Ribbed slab (model 2)

The modelling of the composite slab with the ribs is also considered. For ADAPTIC, the property of geometric orthotropy (i.e. ribs in one direction) is realised by a newly developed flat shell element which is a 4-noded composite/concrete slab element with additional rib and cover freedoms. It deals with the nonlinear analysis of composite floor slabs, enabling the modelling of material nonlinearity and geometric

8

orthotropy through a modification of the Reissner-Mindlin hypothesis. The ribbed case is considered with the following parameters:

- The slab is modelled as a ribbed slab.
- The slab has planar restraints and it is vertically supported along the four edges, while it is free to rotate at its boundaries.
- A full nonlinear response is assumed for concrete and steel.
- The secondary beams are not included.

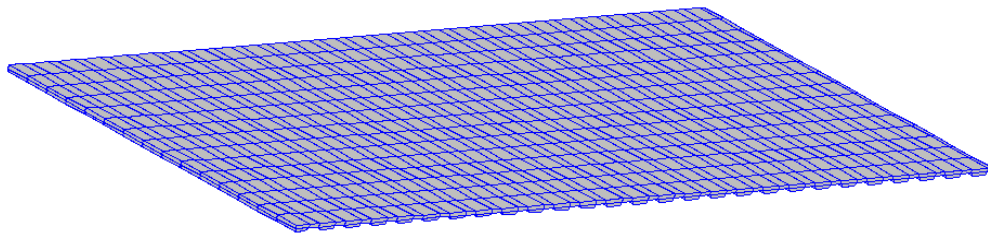The configuration of the ribbed slab model in ADAPTIC is shown in Figure 8.

Fig. 8 The ribbed model in ADAPTIC

In SAFIR, the ribbed slab is modelled by shell elements of height 70 mm in addition to concrete rebars of 30 000 mm²/m in the rib direction. The concrete rebars, which approximate the rib, are positioned at distance 98.4 mm from the top of the slab. The steel deck is modelled as an additional reinforcement mesh of 900 mm^2/m in the rib direction and 0 mm^2/m in the cross direction, positioned at mid-height of the rib (i.e. at distance 100mm below the slab top).

II.3.3 Linear concrete slab (model 3)

In this case, the slab with a linear law of concrete is employed to compare with the reference slab. The model is the same as the reference case except that the full nonlinear concrete material property is replaced by a linear law. The goal of adopting the linear material model is to highlight the importance of concrete nonlinearity in the response of concrete/composite slabs. The variation of material properties (e.g. Young's modulus, Possion's ratio and thermal expansion) with temperature is the same as before.

II.3.4 Slab without planar restraints (model 4)

Two slabs with two different planar restraint conditions are compared. For the slab with planar restraints (reference model), full planar restraints and vertical restraints are applied, hence no axial displacement is permitted for the edge nodes. With regard to the slab without planar restraints, the four edges of slab are free to move inwards but are restrained vertically, in which case the membrane action may still form due to the compression ring within the slab. The edges are free to rotate for both conditions.

The aim of considering different boundary conditions is to check if the planar restraint has significant effects on the load resistance of the considered concrete slab. Through the outcome of this study, the importance of the continuity of composite slabs and the stiffness of the supporting beams along the edges are evaluated.

II.3.5 Slab with secondary beams (model 5)

The effect of secondary beams is also considered. The positions of secondary beams (IPE500) are consistent with the reference building determined for the ROBUSTFIRE project. Vertical and horizontal restraints are applied along the four edges of the slab as well as at the ends of the secondary beams (beams at the edges of the slab are not considered). Under the elevated-temperature conditions, uniformly distributed temperatures over the depth is assumed for secondary beams that have the same material properties of the steel deck, and the temperature linearly increased from the ambient temperature to 900°C. Full shear connection is assumed between the slab and the secondary beams.

The aim of this study is to see if the secondary beams can be beneficial in improving the load carrying capacities of the slab system, particularly under fire conditions. The outcomes of this study can verify one of the assumptions in the proposed '*temperature-independent robustness assessment approach*', which suggests that the fire-affected parts of secondary beams in the fire floor can be directly 'removed' during the analysis. For example, if the response of the slabs with and without secondary beams tends to converge after reaching a certain level of temperature, then the benefits from the secondary beams above this temperature is minimised, and the beams can be considered as removed.

III Results

III.1 Reference case

Figures 9 and 10 give respectively the load-deflection and the deflection-temperature relationships for the uniform thickness slab (reference case) from ADAPTIC and SAFIR. Good correlation is found between the ADAPTIC and SAFIR results. It is worth noting that both of the ambient response curves show a sudden increase in deflection at about 100mm, which is because of concrete cracking. The concrete cracking also leads to the numerical failure of the ribbed slab in ADAPTIC due to a relative high tensile softening slope that is assumed. The early numerical failure can be avoided if a lower tensile softening slope is employed. The deflection shapes of the slab from ADAPTIC and SAFIR (one quarter of the slab) are shown in Figure 11. Figure 12 shows the ambient membrane force in the slab under a UDL of about 18kN/m^2 obtained by SAFIR.
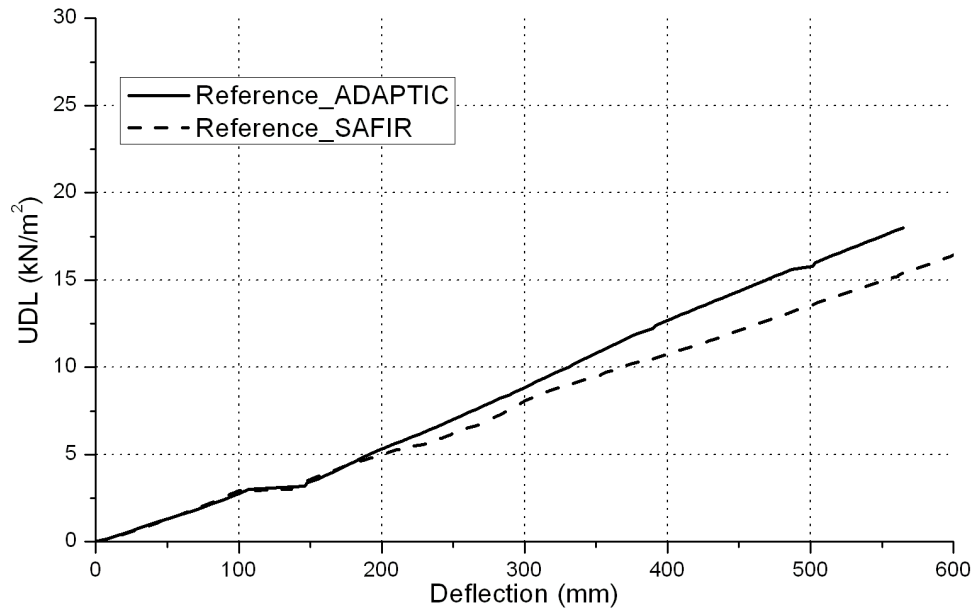
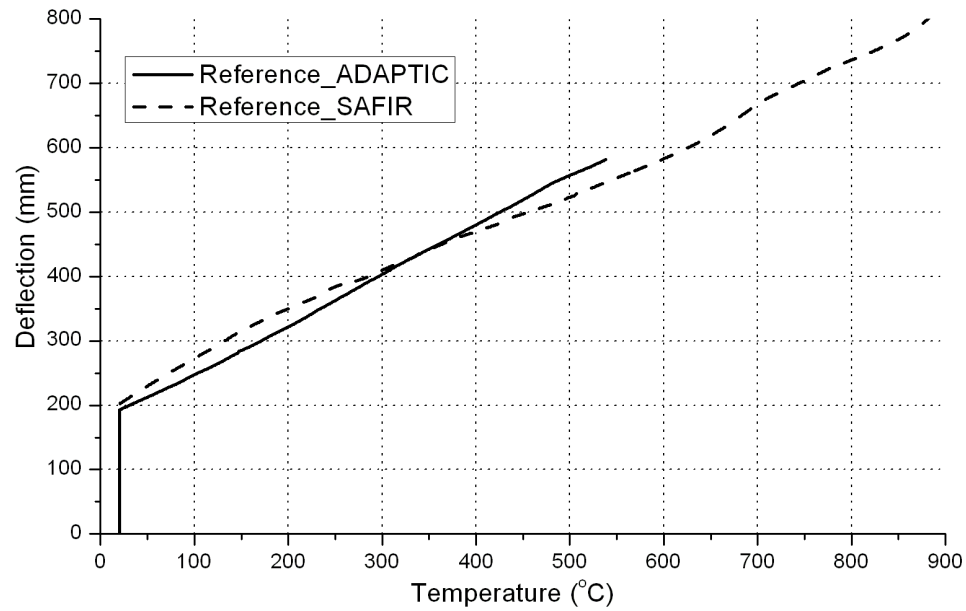Fig. 9 Ambient response of reference (uniform) slab

Fig. 10 Elevated temperature response of reference (uniform) slab
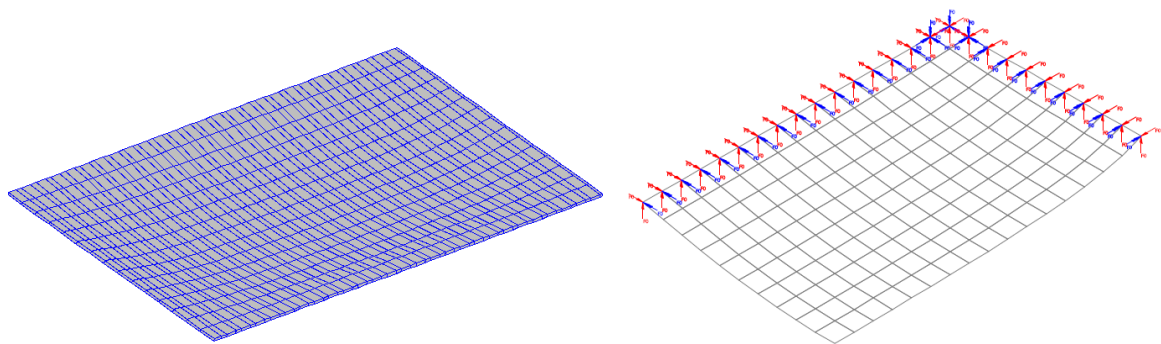

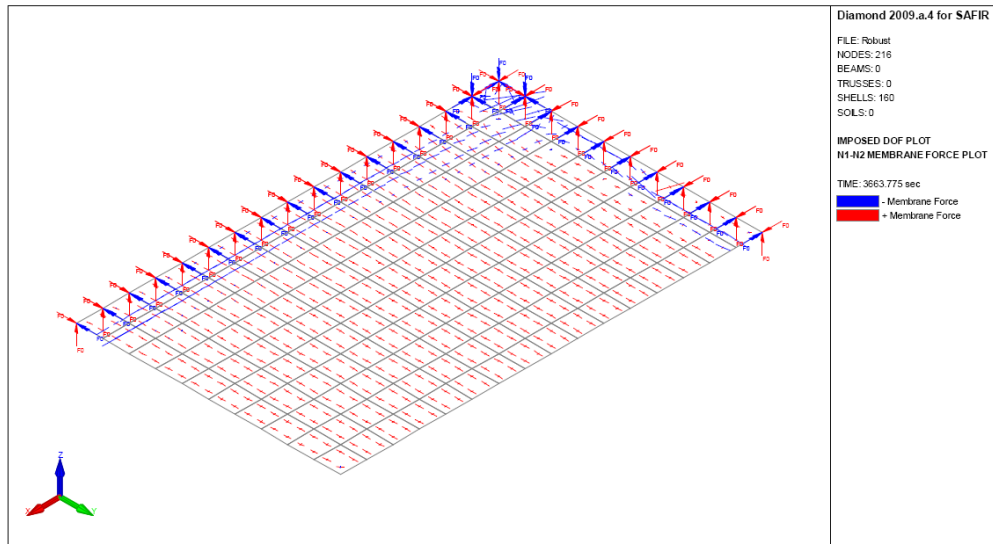Fig. 11 Deflected shapes of slab, left) ADAPTIC, right) SAFIR (one quarter of the slab)

Fig. 12 Membrane forces in SAFIR under ambient conditions (one quarter of the slab)

III.2 Influence of slab profile

Figures 13 and 14 provide respectively the load-deflection and the deflection-temperature relationships for the uniform thickness slab (reference case) and the ribbed slab from ADAPTIC and SAFIR. Good comparisons are found between the ADAPTIC and SAFIR predictions. Some discrepancy is observed in the elevated temperature response, which is attributed to the different modelling approaches employed in the two programs for simulating the ribbed slab profile. It is also found that the ribbed slab has a similar response to the uniform thickness slab with a depth of $d_1+d_2/2$, which indicates that employing uniform slabs with appropriate depths can predict the response of ribbed slabs sufficiently accurately for the considered slab geometry and boundary conditions.
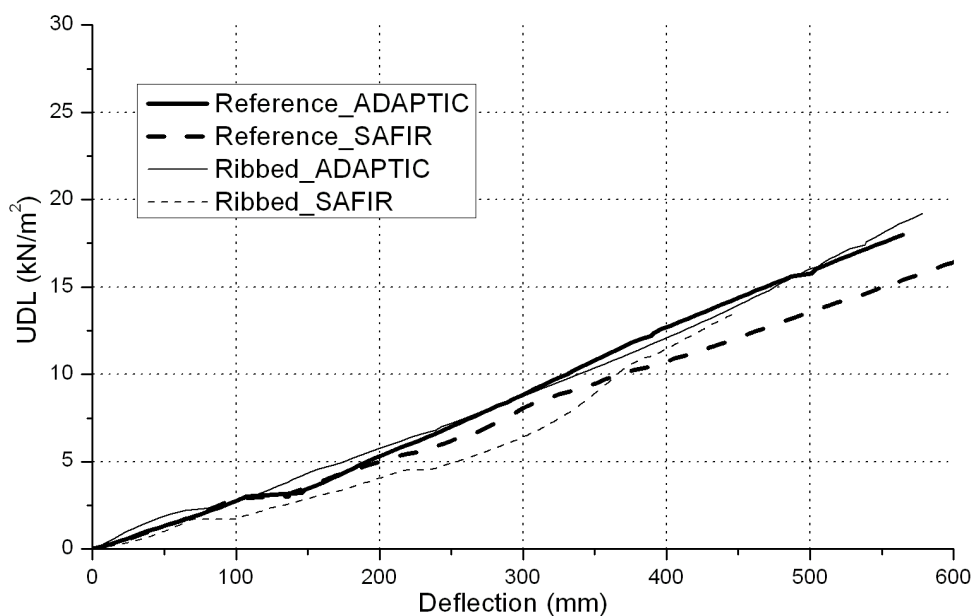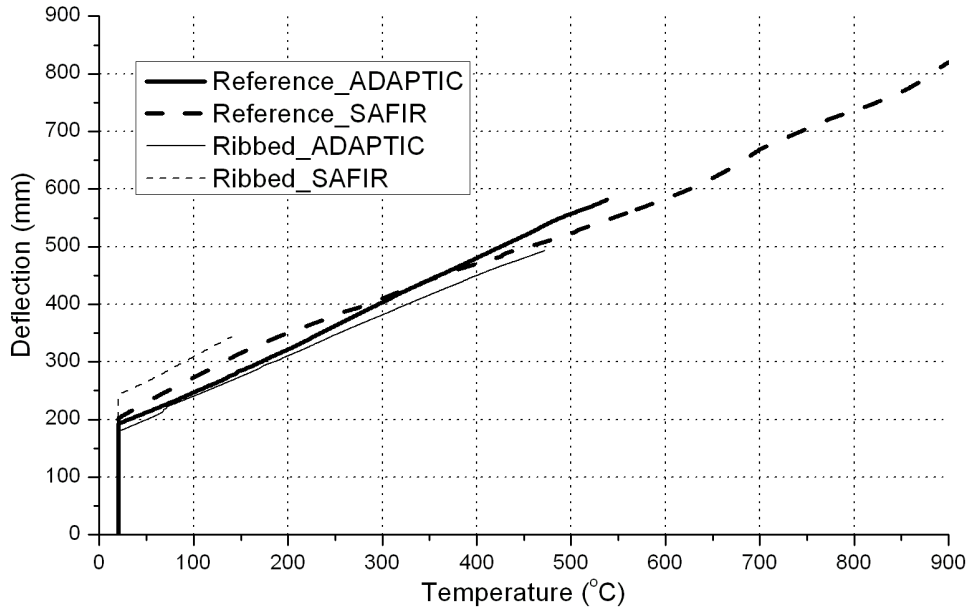

Fig. 13 Ambient response of uniform and ribbed slabs

Fig. 14 Elevated temperature response of uniform and ribbed slabs

III.3 Influence of concrete model

Figures 15 and 16 show respectively the load-deflection and the deflection-temperature relationships for the nonlinear concrete slab (reference case) and the linear concrete slab from ADAPTIC and SAFIR. The ambient responses predicted by the two programs are identical, which implies that the discrepancy found in other cases is mainly due to the different assumptions of the concrete stress-strain relationships. For the elevated temperature condition, the minor discrepancy between the predictions for the linear concrete slab is attributed to a tri-linear material degradation approximation in ADAPTIC, which is different from SAFIR. It is also observed that employing a linear concrete model that ignores the compressive softening, cracking, and tensile softening could lead to unconservative predictions; hence such models should be avoided.
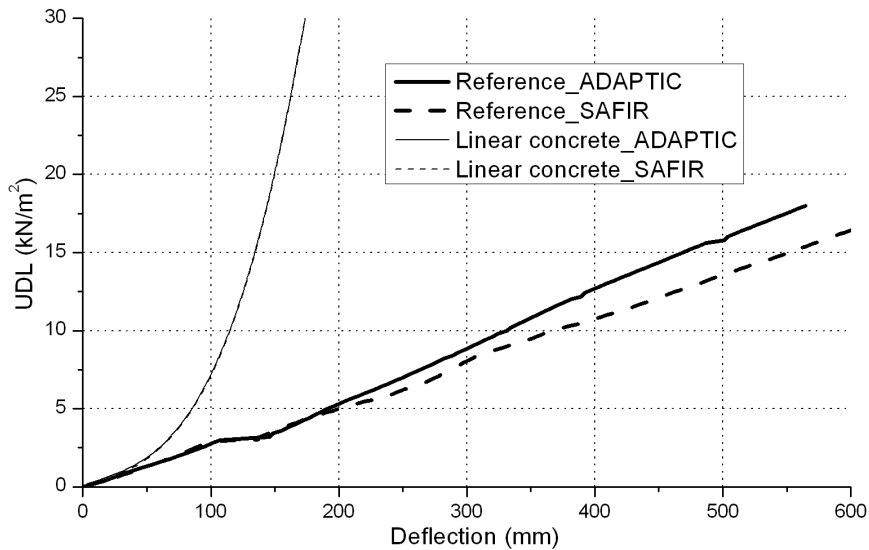

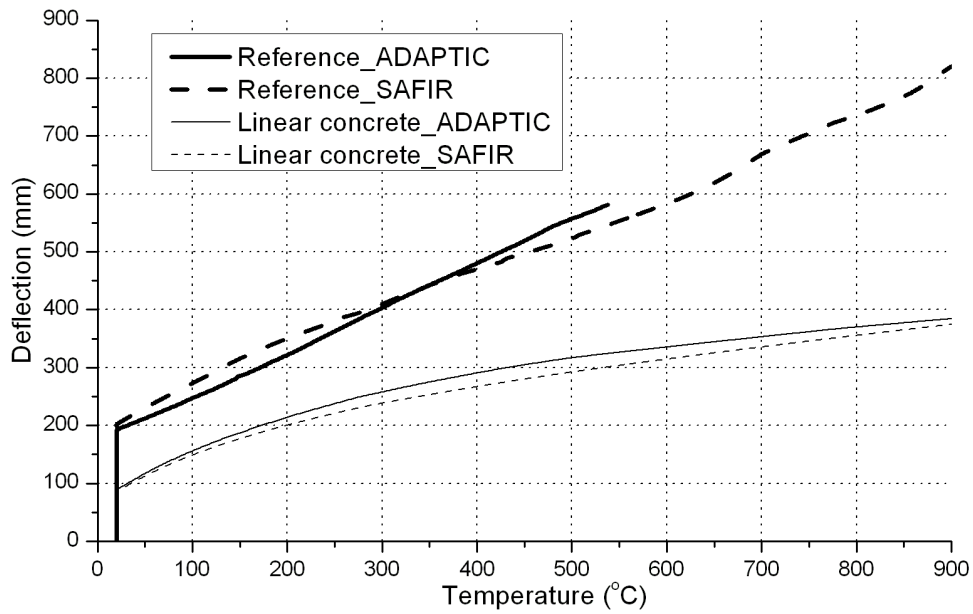Fig. 15 Ambient response of slabs with nonlinear or linear concrete

13

Fig. 16 Elevated temperature response of slabs with nonlinear or linear concrete

III.4 Influence of planar restraints

Figures 17 and 18 provide respectively the load-deflection and the deflection-temperature relationships for the slab with planar restraints (reference case) and the slab without planar restraints from ADAPTIC and SAFIR. Figure 19 illustrates the membrane forces in the slab without planar restraints predicted by SAFIR at ambient temperature. A self-equilibrium mechanism is clearly identified through an outer compressive ring and an inner tension zone. This indicates that membrane action can still be formed in slabs without planar restraints due to the compressive membrane action mechanism. It can be also concluded that planar restraints have a profound effect on the behaviour of concrete slabs. For the ambient condition, the slab with planar restraints can sustain twice the UDL of the slab without planar restraints at a deflection of 200mm, and this value increases to at least four times at a deflection of 600mm. For the elevated temperature situation, an initial deflection of approximately 600mm is predicted by ADAPTIC, but it seems that at this stage the slab is already near collapse, and hardly any temperature loading can be further applied. The initial deflection obtained by SAFIR is relatively larger (about 800mm), and an early numerical failure occurs under 170°C.

As a general comment, although the compressive membrane action can be developed in slabs without planar restraints, the slab load carry capacity is limited for the current configuration. Clearly, better utilisation of tensile membrane action can be achieved with the provision of planar lateral restraints.
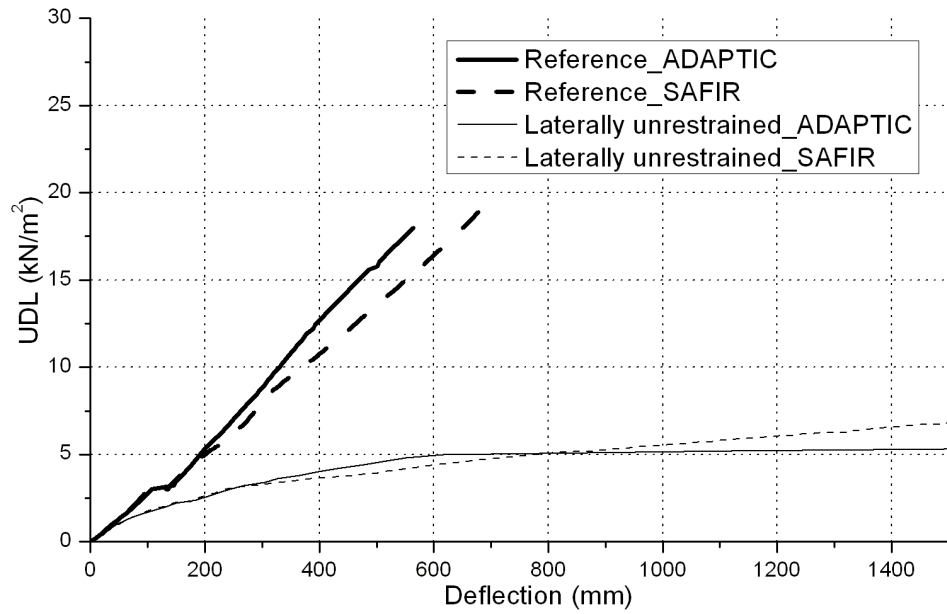
14

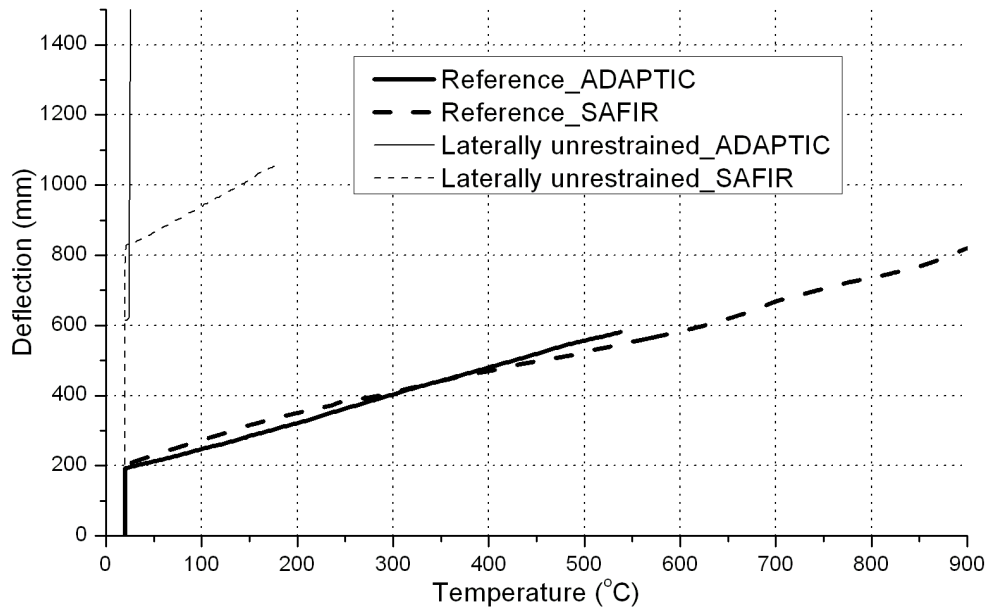Fig. 17 Ambient response of laterally restrained or unrestrained slabs

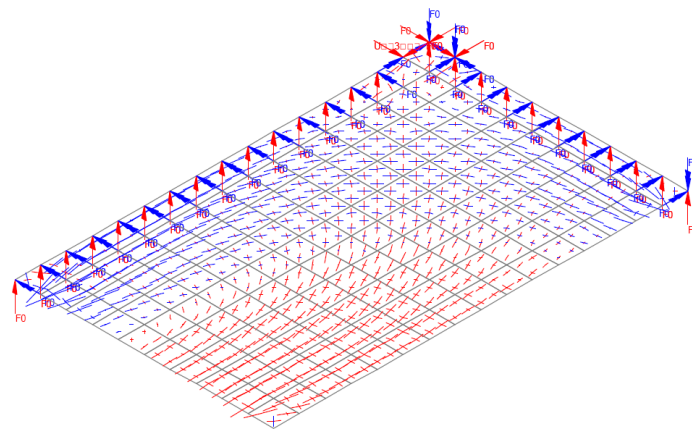Fig. 18 Elevated temperature response of laterally restrained or unrestrained slabs

Fig. 19 Membrane forces in laterally unrestrained slab (one quarter) in SAFIR

15

III.5 Influence of secondary beams

Figures 20 and 21 show respectively the load-deflection and the deflection-temperature relationships for the slab without secondary beams (reference case) and the slab with secondary beams from ADAPTIC and SAFIR. Figure 22 shows the deflected shape of the slab with secondary beams at ambient temperature, under a UDL of 25kN/m^2. Figure 23 provides the membrane forces in the composite slab with and without secondary beams, at ambient temperature under a UDL of 5kN/m^2. It can be seen from this figure that the slab with secondary beams develops a flexural resistance mechanism, while the structure without secondary beams develops a membrane resistance mechanism. As expected, the central deflection of the slab with secondary beams is much smaller than the slab without secondary beams.

The benefit from the secondary beams is maintained until the temperature exceeds a value of approximately 200°C. After this temperature, the deflection of the slab with secondary beams starts to converge with the one without secondary beams, and finally exceeds it as the temperature keeps increasing. This phenomenon implies that at certain stages during a fire, the secondary beams may exert a forcing effect on the load carrying capacity of the slab. This is attributed to the fact that as the temperature increases, secondary beams are in compression due to the thermal expansion induced by the horizontal restraints applied along the edge of the slab. This compressive force accelerates the beam deflection in a buckling type of response, which tends to 'pull' the whole slab system down.
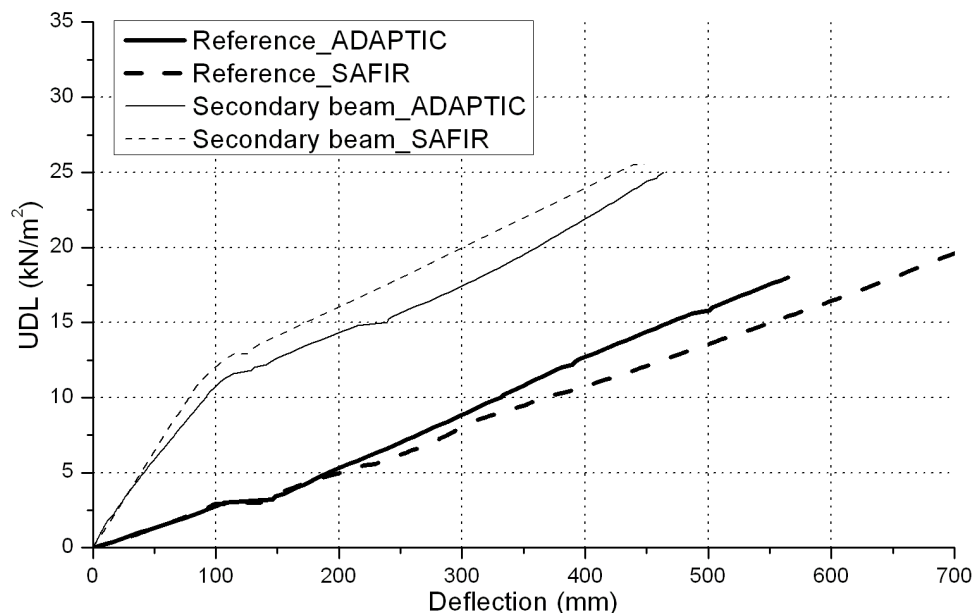

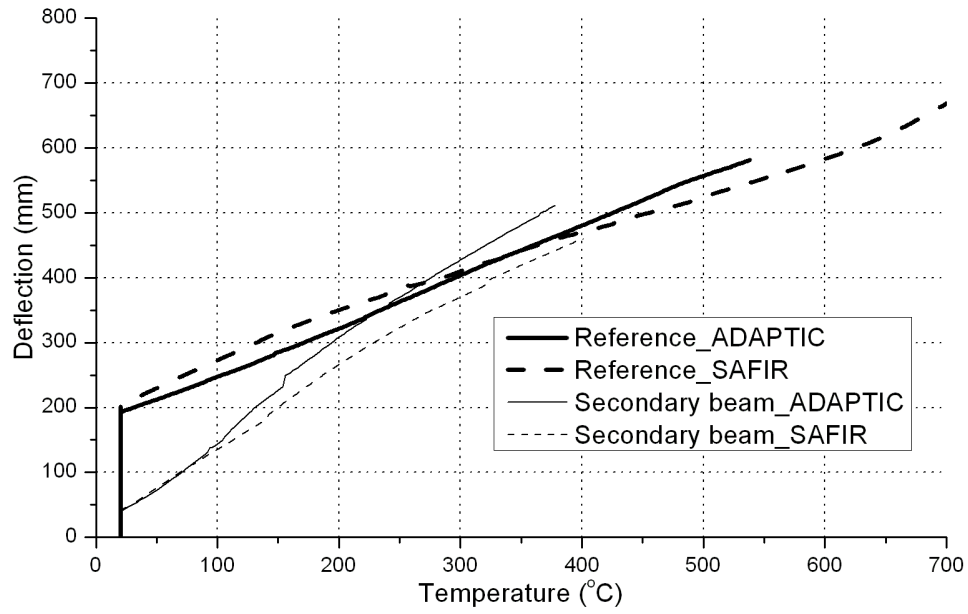Fig. 20 Ambient response of slabs with or without secondary beams

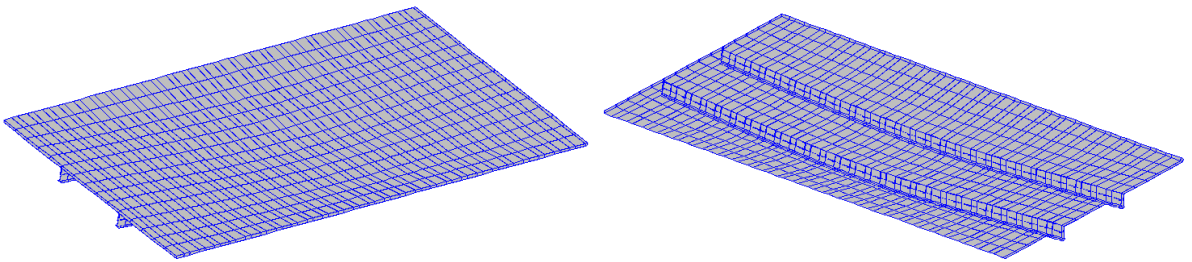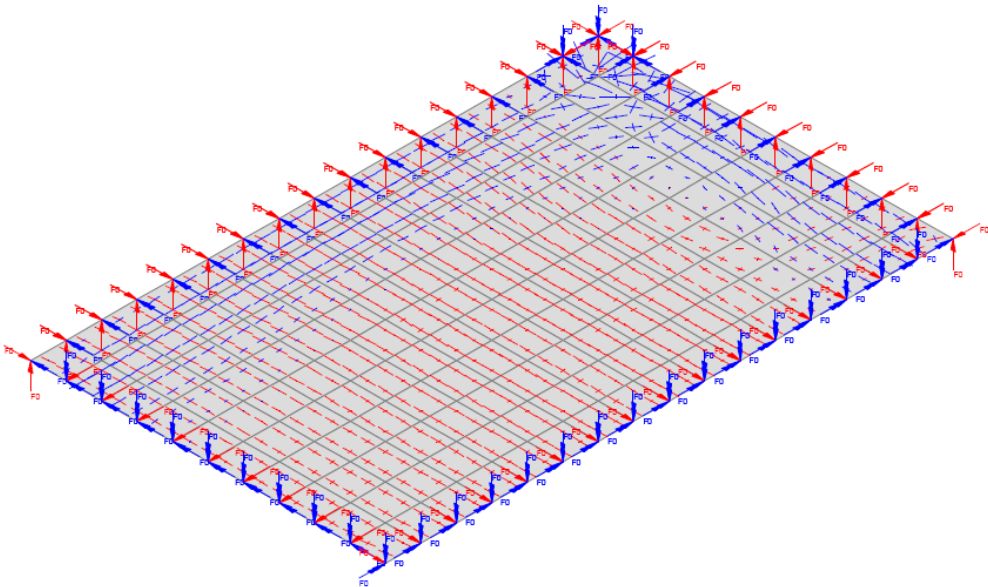Fig. 21 Elevated temperature response of slabs with or without secondary beams

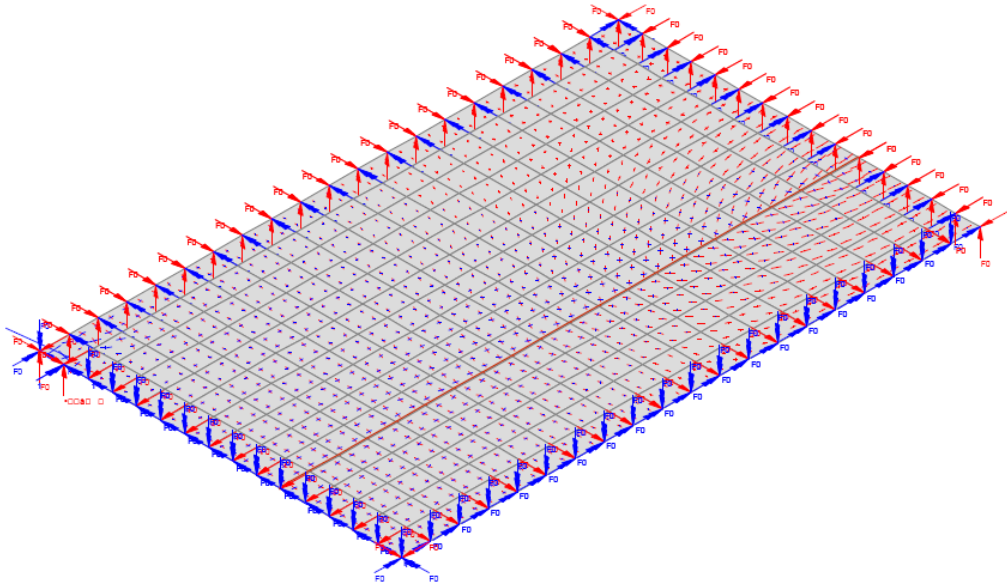Fig. 22 Deflection of slab with secondary beams at ambient temperature in ADAPTIC (UDL= 25kN/m^2)

Fig. 23 Membrane forces of slab (one quarter) at ambient temperature (UDL=5 kN/m²): top) without secondary beams, bottom) with secondary beams

IV Conclusion

The aim of this report is to ensure that the results of slab analysis from the two nonlinear finite element programmes ADAPTIC and SAFIR are comparable, thus to guarantee sufficient accuracy for both programs in modelling the ambient and elevated temperature response of floor systems. In addition, the influence of slab profile, material nonlinearity, boundary conditions and the contribution of secondary beams on the slab response under both ambient and elevated conditions is considered. From the previous discussion, the following conclusions can be drawn:

1) A close comparison is generally found between ADAPTIC and SAFIR, which indicates that the slab response can be predicted with sufficient accuracy using either of the two programs.

2) When the slab is subjected to a large UDL or a high temperature with a thermal gradient, the external loading is typically resisted by membrane action largely via tension in the steel rebars.

3) The ribbed slab model and the flat slab model with an equivalent uniform thickness give similar results. This implies that adopting an equivalent uniform-thickness slab to simulate the ribbed slab can decrease the modelling complexity while potentially maintaining sufficient accuracy.

4) A linear concrete model gives unconservative results, and should therefore be avoided.

5) If a slab has no planar restraints, its stiffness and strength are much lower compared with the same slab with planar restraints. But the slab without planar restraints is still able to sustain considerable load due to the equilibrium mechanism by means of a compression ring within the concrete.

6) The secondary beams are necessary for floor slabs at ambient temperature, but at high temperature their benefit is negligible because the steel loses strength and stiffness. Therefore, the steel beam (or part of the steel beam) subject to high temperature can be 'removed'. Even worse, the combined effects of thermal expansion and thermal bowing may increase the vertical deflection of the beam or lead to a premature member buckling. Consequently, an even larger deflection can be observed for the floor system with secondary beams than the one without secondary beams.

V Reference

ADAPTIC user manual, Version 1.3b, Izzuddin, 2009, March.

EN 1992-1-1:2004. "Eurocode 4: Design of concrete structures - Part 1-1: General rules and rules for buildings". European committee for standardization, December 2004.

EN 1992-1-2:2004. "Eurocode 2: Design of concrete structures – Part 1-2: General rules – Structural fire design". European committee for standardization, December 2004.

EN 1993-1-2:2005. "Eurocode 3: Design of steel structures – Part 1-2: General rules – Structural fire design". European committee for standardization, April 2005.

EN 1993-1-1:2005. "Eurocode 3: Design of steel structures - Part 1-1: General rules and rules for buildings". European committee for standardization, May 2005.

EN 1994-1-1:2004. "Eurocode 4: Design of composite steel and concrete structures – Part 1-1: General rules and rules for buildings". European committee for standardization, December 2004.

EN 1994-1-2:2005. "Eurocode 4: Design of composite steel and concrete structures – Part 1-2: General rules – Structural fire design". European committee for standardization, 2005.

Elghazouli, A.Y., and Izzuddin, B.A. (2004a) Realistic Modeling of Composite and Reinforced Concrete Floor Slabs under Extreme Loading. Part II: Verification and Application. Journal of Structural Engineering, ASCE, 130(12), 1985-1996.

Izzuddin, B.A. (1991) Nonlinear Dynamic Analysis of Framed Structures. PhD Thesis. Department of Civil Engineering, Imperial College, University of London, London, UK.

Izzuddin, B.A., Tao, X.Y., and Elghazouli, A.Y. (2004) Realistic Modeling of Composite and Reinforced Concrete Floor Slabs under Extreme Loading. Part I: Analytical Method. Journal of Structural Engineering, ASCE, 130(12), 1972-1984.

ANNEX B

Departamento de Engenharia Civil

Faculdade de Ciências e Tecnologia da Universidade de Coimbra

ROBUSTFIRE Project

Document 8: FEM simulation of sub-frame

Cécile Haremza

Aldina Santiago

Luís Simões da Silva

January 2012

Table of contents

I. Introduction

This work presents a finite element model developed to study the behaviour of a composite steel-concrete sub-frame. The commercial general finite element package Abaqus (2011) is used to model the composite steel-concrete beam-to-column frame extracted from the real open car park building. The symmetry of the joint is taken into account, and the structural elements are modelled combining C3D8R solid elements and contact pairs. The main objective is to study the detailed behaviour of the composite sub-frame when it is subjected to the loss of a column in the car park building. Materials for steel members and connection components are established by the steel tensile coupon tests, whereas the concrete behaviour is defined according to Eurocode 2 part 1.1 (EN 1992-1-1:2004). The behaviour of the joint under bending moments is discussed: first, numerical results for the steel frame under hogging and sagging bending moments are shown (the "steel model"); then, preliminary results for the composite steel-concrete frame under sagging bending moment (the "composite model") are presented and compared with the results of the experimental test that was performed at the University of Coimbra at ambient temperature (reference test 1).

II. The experimental test

In this paper, only the reference test performed at ambient temperature (see WP2) is presented. The real cross-section dimensions were kept in the laboratory (Figure 1a): two composite beams with IPE550 steel cross-sections, grade S355, one column HEB 300, grade S460, and bolts M30, cl 10.9. In order to ensure the composite behaviour of the beam-to-column joint, ten steel rebars of diameter 12 mm were placed in the composite slab at each side of the column. The steel beam was fully connected to the composite slab by 22 shear studs (diameter = 19 mm; height = 100 mm). Because of the restrictions from the laboratory dimensions, the beam length was reduced from 10 m in the real building to 3 m in the sub-structure to be tested.

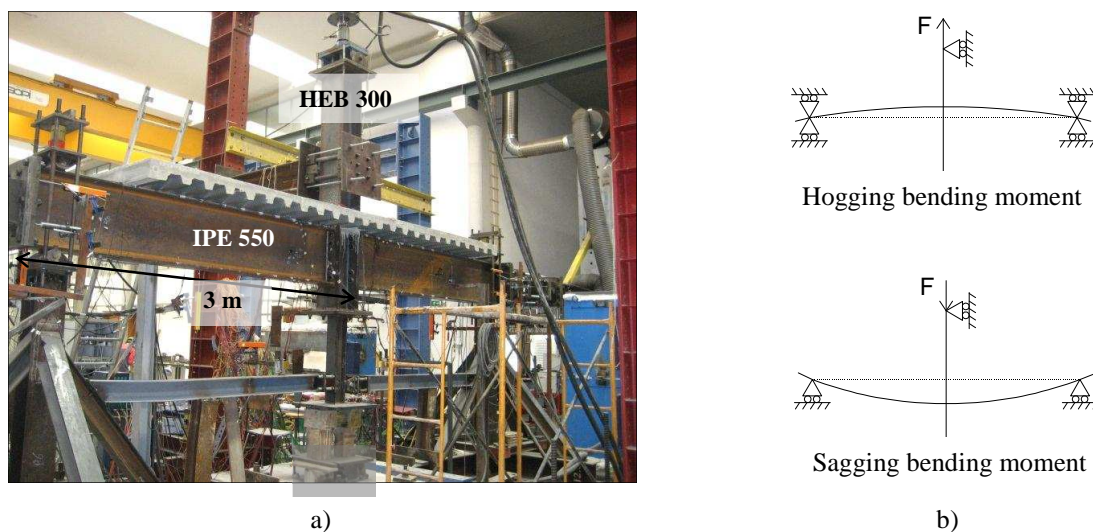a)   b)

Figure 1. a) Outline of the experimental test; b) Loading sequence: initial hogging bending moment, followed by the increase of the sagging bending moment after the column loss

The test was divided into 2 main steps: step 1 - application of an initial hogging bending moment in the joint, and step 2 - increase of the sagging bending moment up to the failure of the joint. Step 1 simulated the internal loads in the connection as in the actual car park; a hogging bending moment equal to -450 kNm was applied in the joint. This bending moment in the joint was applied by increasing the vertical load at the column top in the upward direction whereas the vertical displacements of the beam extremities were locked and the vertical displacement of the joint was free (see Figure 1b)). Then, the vertical load at the column top was increased in the downward direction in order to increase the sagging bending moment in the joint and to reach the sub-frame failure (step 2). During the increase of the sagging bending moment, the column was assumed to be completely failed.

III. The numerical model

The commercial general finite element packages Abaqus is used to perform the numerical simulations of the steel and composite frame subjected to variable bending moments at ambient temperature. The mechanical properties of the material steel, bolts and concrete, as well as the general modelling assumptions are detailed in this section.

III.1. Mechanical properties

III.1.1. Steel properties (beam, column and end-plate)

Mechanical properties of the steel from the beam, the column and the end-plate are defined by tensile coupon tests. From the steel profiles, the coupons were extracted from the webs and flanges, and three tensile tests were performed for each. In the case of the steel end-plate, only two coupons were performed and tested. Figure 2 shows the standardized curves that were defined using the Menegotto-Pinto model (for materials of sharp-knee type), in Kato, 2010, based on the stress-strain curves from the tensile tests.
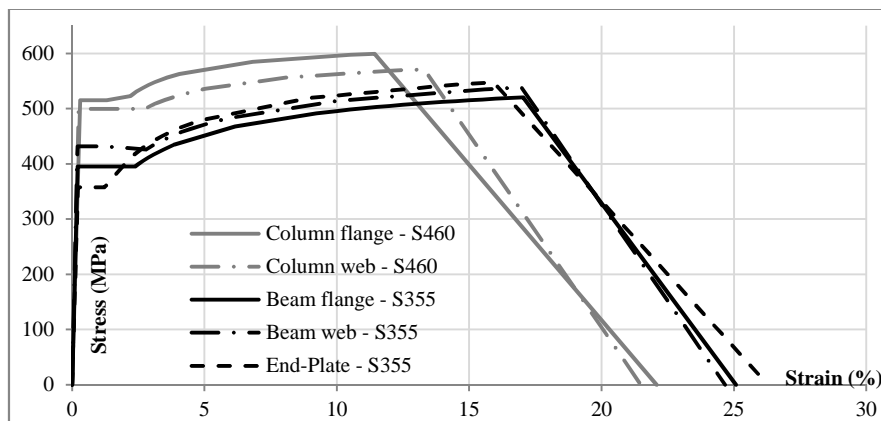

Figure 2. Stress-strain curves of steel from the webs and flanges of columns HEB 300 (S460) and beams IPE 550 (S355), and from the end-plate (S355 - 15 mm thickness)

For Abaqus simulation, the nominal stress-strain values $(\sigma_{nom}, \varepsilon_{nom})$ obtained from the standardized curves (Figure 2) are converted to the true stress-strain measures $(\sigma_{tru}, \varepsilon_{tru})$ calculated by equation (1) (Malvern, 1969):

$$\sigma_{tru} = \sigma_{nom}(1 + \varepsilon_{nom}) \qquad \text{and} \qquad \varepsilon_{tru} = \ln(1 + \varepsilon_{nom}) \tag{1}$$

III.1.2. Properties of M30 grade 10.9 bolts

Two tensile tests were performed on coupons extracted from bolts at ambient temperature. The nominal stress-strain curves obtained from the tensile tests are idealized by a bi-linear curve with a yield strength equal to 932 MPa ($\varepsilon_{nom} = 0.45$ %) and the ultimate tensile strength equal to 1044 MPa ($\varepsilon_{nom} = 5$ %). The true stress-strain values are defined by the previous equation (1) and are used in Abaqus.

III.1.3. Concrete properties

Concrete properties are defined according to Eurocode 2 part 1.1, and the stress-strain behaviour of the concrete C25/30 in compression is shown in Figure 3. Compression tests on concrete cubes were performed after 7 days, 14 days, 28 days and the day of the experimental test. The concrete properties C25/30 at 28 days were confirmed according to NP EN 206-1 2007: i) the average of each three tests cube strength (fck,cube = 35 MPa) is higher than the C25/30 characteristic cube strength plus 1 (31 MPa) and is smaller than the C30/37 characteristic cube strength plus one (38 MPa); ii) each individual value is higher than the C25/30 characteristic cube strength minus 4 (26 MPa).
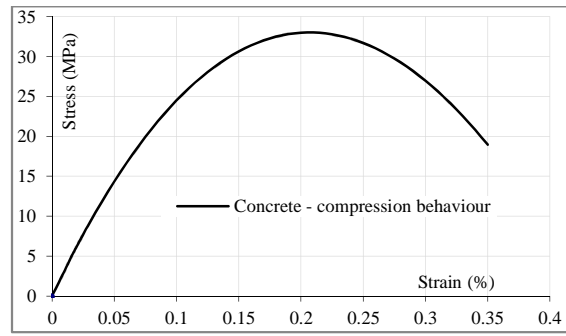
Figure 3. Stress-strain behaviour of the concrete in compression

The behaviour of the reinforced concrete in tension is defined by the maximum tensile stress (2.6 MPa), and by its fracture energy G_F (93.4 N/m), defined by the equation (2) (CEB, 1990).

$$G_F = G_{F0} \left(\frac{f_{cm}}{10}\right)^{0.7} \qquad (2)$$

where f_{cm} is the mean value of concrete cylinder compressive strength defined in Eurocode 2 (33 MPa), and G_{F0} is the base value of the fracture energy (40.5 N/m), depending of the largest nominal maximum aggregate size (22 mm in this case).

III.2. General modelling assumptions

In order to save computational time, the symmetry of the joint is taken into account in the model; only one fourth of the column, half of the end-plate, four bolts and one fourth of the concrete slab are modelled. The displacements out of the plane (z-direction in Figure 4) of the column web and beam web are restrained, assuming no local buckling of the webs. This assumption is made according the evidence of the deformed frame after the experimental test. The main joint members are modelled with three-dimensional 8-node linear brick, reduced integration solid elements (C3D8R). In order to simplify the model and save computational time, the upper part of the steel column away from the joint zone is modelled using general B31 beam elements. The Abaqus "Coupling" function joins these two finite elements (Dai, 2010). The measured initial deformation of the end-plate (space of 0.6 mm between the end-plate centre and the column flange) is reproduced in Abaqus using a sinusoidal shape between bolt rows 2 and 3. Because the purpose of this study is the joint behaviour, no geometrical imperfections are introduced in the beam and in the column. Bolts M30 are modelled with a reduced diameter size d_s equal to 26.73 mm, equivalent to the resistant section A_s (561 mm2). In order to simplify the model and avoid some numerical convergence problems, the hole around the bolt shank (diameter of 26.83 mm) is only slightly higher than the bolt diameter (EN 1090-2:2008). Bolt head and nut are modelled circular and include the two washers that were used during the tests; the bolt threads are not modelled (see Figure 5).

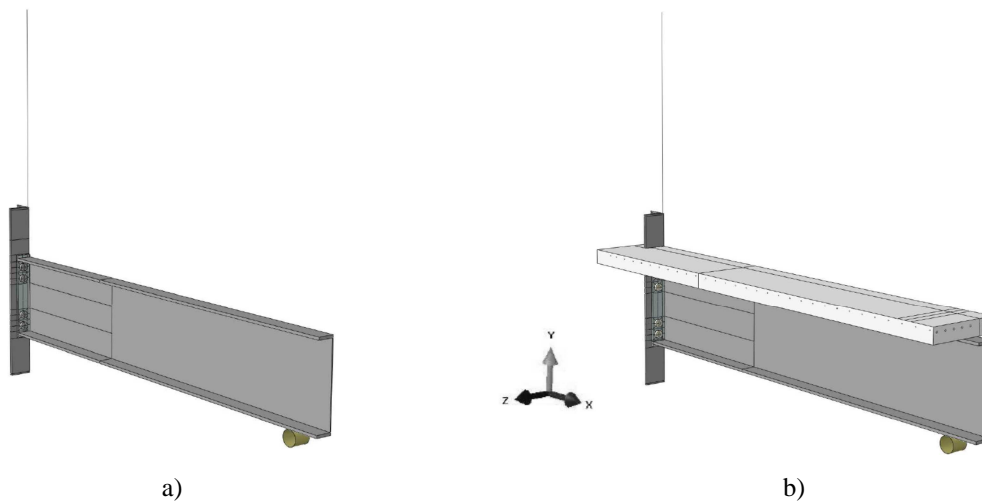a)   b)

Figure 4. 3D FE model of the steel (a) and composite steel-concrete (b) frame in Abaqus

For the composite model, the composite slab is simplified by a concrete slab, with an equivalent rectangular section of thickness 94 mm and width 450 mm. It is assumed that the concrete from the ribs

5

(total height of 130 mm) is uniformly allocated to the entire slab. The five steel rebars of 12 mm diameter, as well as the constructional longitudinal (8 mm diameter) and transversal rebars (6 mm diameter), are modelled with solid elements and are embedded in the concrete slab (see Figure 5). In order to prevent sliding, the full connection between the concrete slab and the steel beam is modelled using the TIE option. However, as this TIE full connection does not allow any sliding, once the frame starts deforming, unrealistic high tensile stresses appear at the surface of the concrete slab in contact with the steel beam, which making it difficult for the model to converge. These tensile stresses should be avoided, and the shear connectors should be modelled in order to simulate the realistic sliding behaviour.

Welds are not modelled and the steel beam is fully connected to the end-plate using the TIE option. Contact interactions are defined between the end-plate and the column flange, and between each bolt and the column flange and the end-plate: nut - column flange; bolt head - end-plate; bolt shank - column flange hole; bolt shank - end-plate hole. Contacts are defined as surface-to-surface contact with a small sliding option. Normal contact is defined as "hard contact" with default constraint enforcement method, and separation is allowed after contact. A friction coefficient of 0.25 is used in the tangential behaviour with penalty friction formulation. A contact surface is also defined between the concrete slab and the steel column (hard contact allowing separation after contact and frictionless). The bolts and the end-plate are meshed similarly, whereas the column has a coarser mesh (see Figure 5).
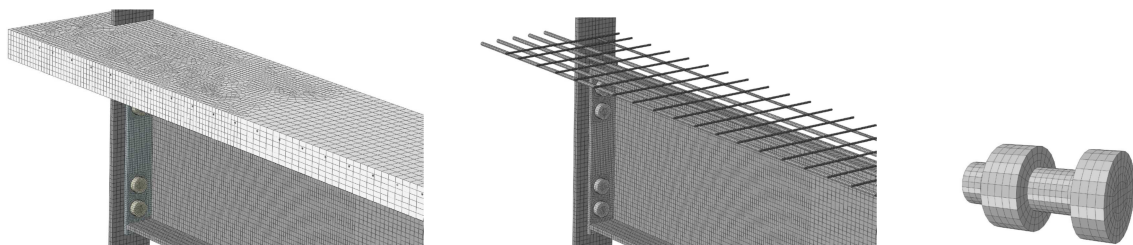

Figure 5. 3D meshed FE model of the steel and composite frame in Abaqus, including the rebars detail

The general static analysis is used. Several steps are defined: step 1 - pre-loading of bolts; step 2 - application of the self-weight; step 3 - hogging bending moment; steps 4 and 5 - sagging bending moment. In order to improve the convergence of the model, an artificial viscous damping is also defined for each step. This artificial damping is defined in Abaqus via the dissipated energy fraction (0.0002), and it is verified that the ratio of the dissipated energy by damping to the total strain energy does not exceed 10%. The static analysis algorithm is really difficult to solve once contact pairs are defined, and an easy way to pass through the first step is to pre-load the bolts at the beginning of the analysis, using the "Bolt load" option. The adjust length method is applied for each bolt (adjust of 0.07 mm), which reproduces the pre-loading applied in the test (about 120 kN). During the application of the pre-load, displacements of the bolt heads and of the steel end-plate are restrained.

The y-direction at the beam extremity is restrained during steps 1 to 3; during the application of the sagging bending moment (steps 4 and 5), the support is modelled by a rigid cylinder in contact with the beam, no friction is applied (Figure 4). The x-direction beam extremity is free; the top of the column is free in the y-direction, and the x and z directions are restrained all along the column. The application of the hogging and sagging bending moments in the joint are simulated by displacement control at the top of the column.

IV.   Numerical and experimental results

The comparison between the results from the experimental test and FE models is made based on the Force-Displacement and the Moment-Rotation curves. The applied load at the column top (see Figure 1b) and the vertical displacement of the joint define the force-displacement curve. The bending moment and rotation values are deducted from the FE model as for the experimental test: the joint rotation was estimated using the vertical displacements measured at 1500 mm from the plate (D002 in Figure 6), and at the column (D028 in Figure 6) and the bending moment is calculated using the reaction load at the beam support.
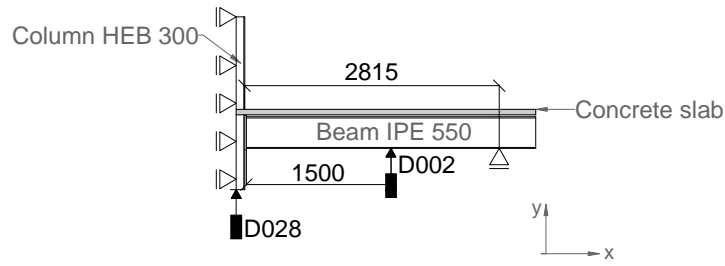
Figure 6. Schematic frame modelled in Abaqus

IV.1. *Results of the experimental test*

The evolution of the total load applied at the column top versus the vertical displacement of the joint, and the bending moment versus the rotation of the left connection are depicted in Figure 7. The hogging bending moment was initially reached during step 1 (about -500 kNm), by increasing a vertical load (-351 kN) at the column top in the upward direction. During the step 2, the load increased in the downward direction and the sagging bending moment increased.
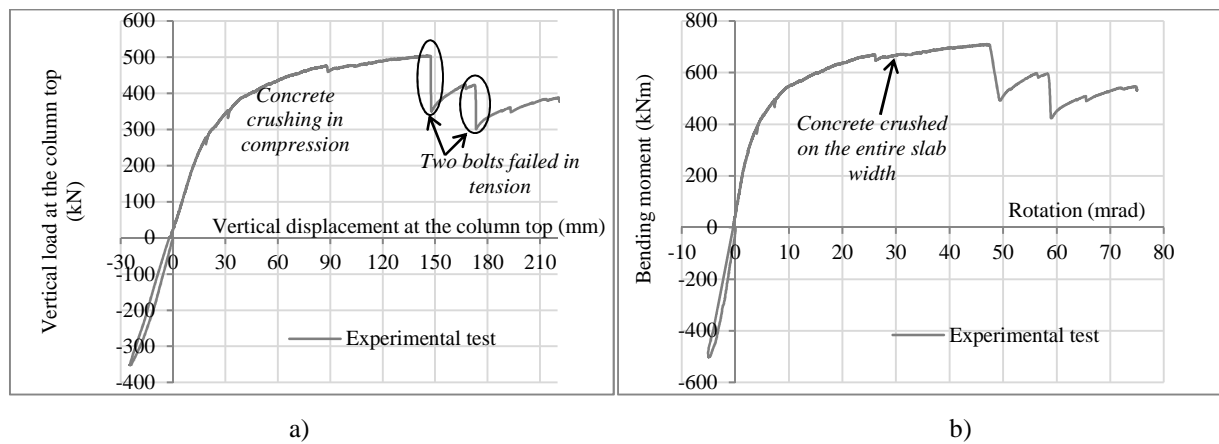

Figure 7. a) Applied load at the column top vs vertical displacement of the column; b) Bending moment vs rotation at the joint left side

Concrete crushing in compression was the first failure observed, but this failure was really progressive and cannot be identified on the force-displacement / moment-rotation curves (Figure 7). At about 30 mrad of rotation, the concrete from the composite slab was crushed on the entire slab width. One first bolt suddenly failed after 148 mm of joint vertical displacement and the applied load reduced from 503 kN to 351 kN. The corresponding bending moment was reduced from 707 kNm to 494 kNm, and the rotation increased from 47.5 mrad to 49 mrad on the left side because of the sudden slight rotation of the column once the bolt failed. The deformation of the left side of the joint and the one of the right side began to differ, notably because of the slight column rotation. A second bolt failed under a load equal to 393 kN, with a vertical displacement equal to 173 mm (which correspond to 554 kNm of bending moment and 59 mrad of rotation on the left side). Figure 8 presents the final deformations of the joint at the end of the experimental test, after the failure of the two bolts. The failed bolts were identified: i) in the bottom bolt rows - because of higher tensile forces under sagging bending moment, and ii) in the left connection due to a slight asymmetric joint deformation. Finally, the test was stopped at 75 mrad and 68 mrad of connection left and right rotations. Due to high stresses/deformations, a crack at the base steel end-plate, just above the weld, appeared at the end of the test. Moreover, the new localised deformation mode was observed at the steel end-plate centre.
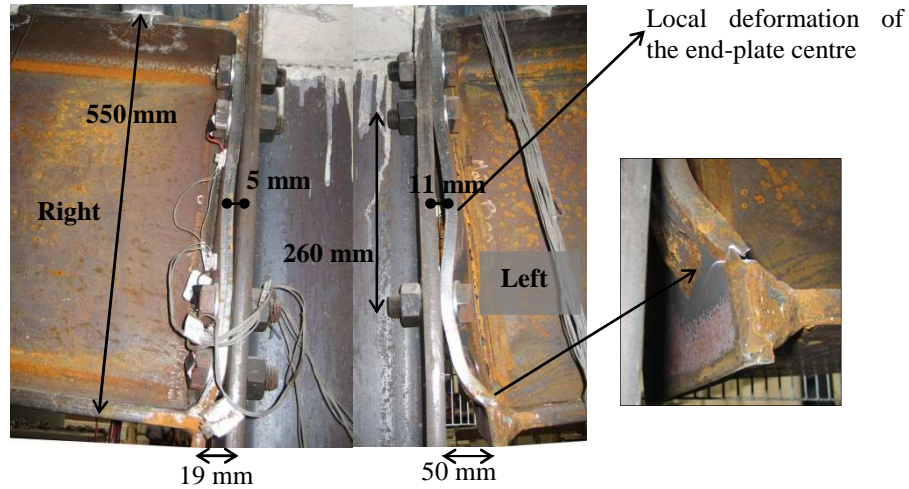
Figure 8. Deformations of the joint (view from the back side)

IV.2. *Results of the FE models and comparisons to the experimental test*

IV.2.1. Results of the FE steel model

The numerical and experimental bending moments / rotations curves are compared in Figure 9. The FE steel model reached a hogging bending moment equal to -244 kNm and a maximum sagging bending moment equal to 507 kNm, which corresponds to a maximum rotation of 33 mrad.
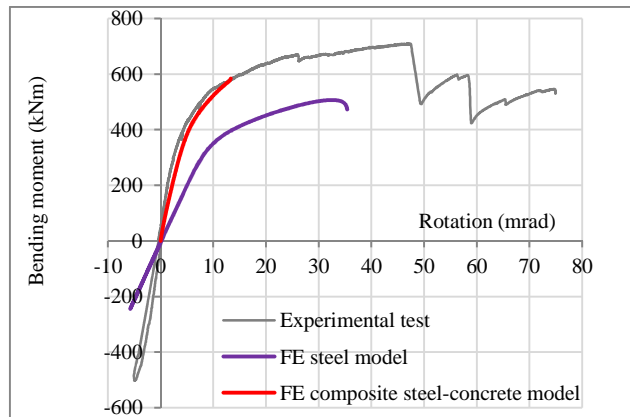

Figure 9. Bending moment vs rotation at the joint left side – Comparisons between experimental and FE results

Figure 10a) and b) show the Von Mises stresses in the beam and in the two bottom bolts (rows 3 and 4), under the maximum bending moment (507 kNm). Plastic deformations of the end-plate are evidenced in the compression zone, and the ultimate stress-strain is reached in the bottom bolt (row 4). Once this bolt failed, the bending moment begin to decrease and the FE model end because of non-convergence. Equivalent plastic strains in the bottom bolt (Figure 10c)) are located near the bolt head, just like the bolt failure during the experimental test.
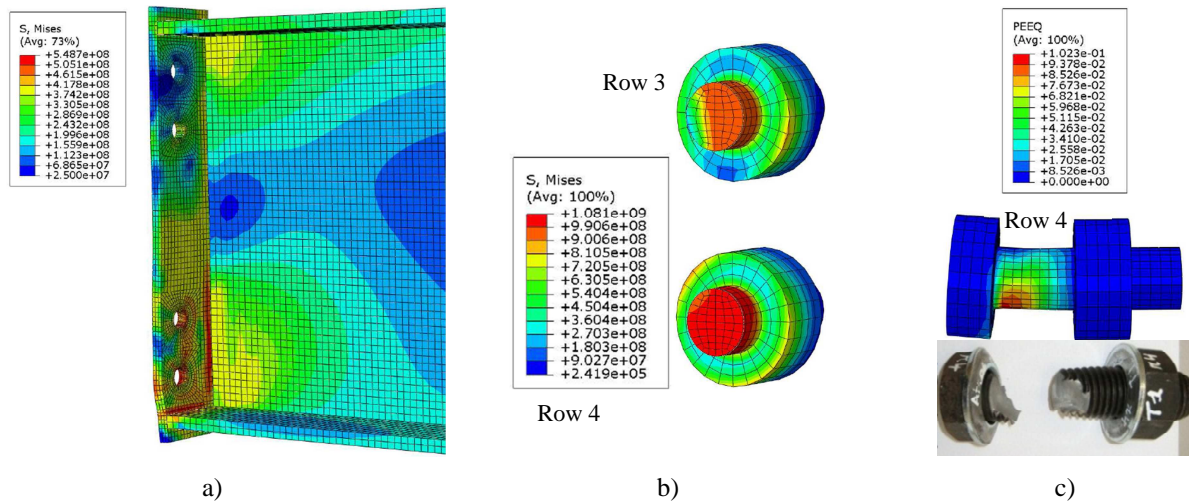
8

Figure 10. Calculated values (N/m2) at the maximum load of the steel model: a) Von Mises stresses in the beam and end-plate; b) Von Mises stress in bolts from the two bottom bolt rows (3 and 4); c) Location of the bolt failure and equivalent plastic strains

The comparison between the experimental test and the steel model shows that the main advantages of the concrete slab are the increase of: i) the initial stiffness, more 70% and 95% under sagging and hogging bending moments respectively; and ii) the resistance, the first failure of the bolt happens latter, and the maximum sagging bending moment is increased of 40%.

IV.2.2.   Results of the FE composite model

The initial stiffness of the FE composite model is 23% higher than the stiffness obtained from the experimental test (Figure 9). The behaviour of both under sagging bending moment (experimental test and FE model) is very similar and close. Figure 11a) and b) present the Von Mises stresses in the beam and in the two bottom bolts (rows 3 and 4) under the last increment (bending moment equal to 584 kNm, and rotation equal to 13.3 mrad). The bolt has not yet reached the ultimate stress-strain. Figure 11c) shows that the equivalent plastic strains in the bottom bolt (row 4) are localised near the bolt head (as observed in the steel model). At this point (13.3 mrad), the concrete is not yet crushed against the column flange. However, in the experimental test, the concrete was crushed against the column flanges for 13/14 mrad of rotation.
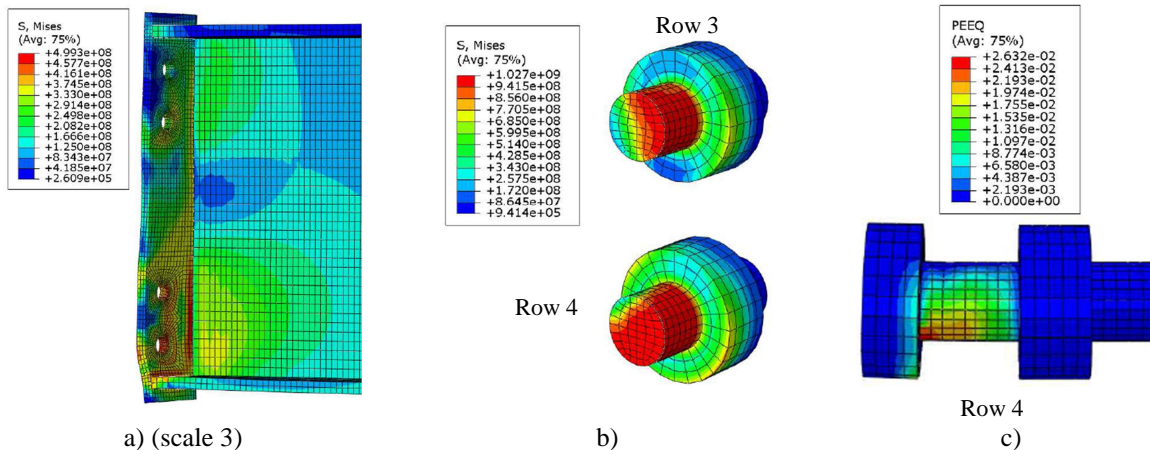

Figure 11. Calculated values at the last increment of the composite FE model: a) Von Mises stress in the beam and end-plate; b) Von Mises stress from the two bottom bolt rows (row 3 and row 4); c) Equivalent plastic strains in the bolt (row 4)

The deformation mode under sagging bending moment for the FE steel and the composite models are compared in Figure 12 to the experimental deformations obtained at the end of the test, which do not correspond to the same level of loading; deformation modes are similar. The deformation at the end-plate centre do not appear as high as the experimental test, but it is not quantitative comparable for now because: i) the maximum deformation of the frame in the experimental test is higher than for the FE

9

models, and ii) the hole in the end-plate and column flange for the shank of the bolt is not modelled as in reality, with more 3 mm for the diameter defined in EN 1990-2:2008 for bolts M30.
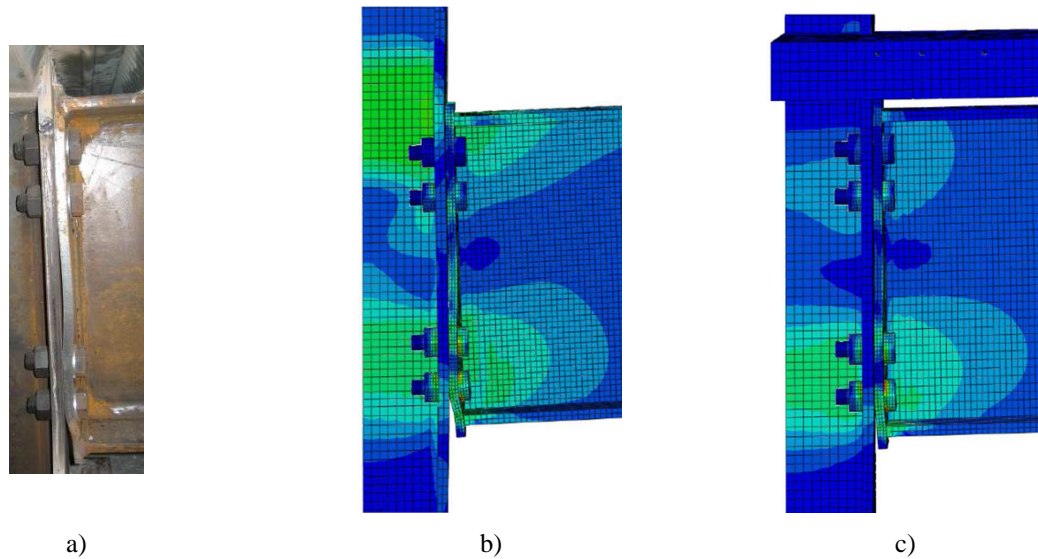

a)　　　　　　　　　　b)　　　　　　　　　　c)

Figure 12. End-plate deformation at: a) the end of the experimental test (vertical displacement of 220 mm); b) the steel model (vertical displacement of 104 mm); c) the composite model (vertical displacement of 39 mm)

V. Conclusions

This work presented the results of a detailed three-dimensional FE model that simulates the effect of the loss of a column in a composite steel-concrete beam-to-column sub-frame, using the non-linear finite element package Abaqus, 2011. The FE model was calibrated against the experimental test subjected to variable bending moments, at ambient temperature. The behaviour of the steel sub-frame obtained from the FE model, and the behaviour of the composite sub-frame under sagging bending moment were presented and compared to the experimental test results; good agreement was observed. The convergence of the composite model could be improved, notably by an appropriate definition of the damping energy, but also by modelling: i) the shear connectors between the concrete slab and the steel beam; ii) a higher bolt hole in the end-plate and in the column flange (in order to observe if the 3 mm space would influence the centre deformation of the end-plate under sagging bending moment).

VI.　References

Abaqus (2011). Analysis User's manual, v6.11, Dassault Systems Simulia Corp., Providence, USA.

Comité euro-international du béton (1990). "CEB-FIP – Model Code", Design code, Thomas Telford Services Ltd.

Dai X.H., Wang Y.C., Bailey C.G. (2010). "Numerical modelling of structural fire behaviour of restrained steel beam-column assemblies using typical joint types", Engineering Structures, Vol. 32, 2337-2351.

Demonceau J.F. (2009). "ROBUSTFIRE Project - Design of the joints - notes", Internal document, University of Liège.

EN 1090-2:2008, "Execution of steel structures and aluminium structures, Part 2: Technical requirements for steel structures", 2008.

EN 1992-1-1:2004, "Eurocode 2: Design of concrete structures - Part 1-1: General rules and rules for buildings", European committee for standardization, December 2004.

Gens F. (2010). "ROBUSTFIRE Project - Pre-dimensionning of the reference's car park", Internal document, Greisch.

Kato B., Aoki H., Yamanouchi H. (1990). "Standardized mathematical expression for stress-strain relations of structural steel under monotonic and uniaxial tension loading", Materials and Structures/Matériaux et Constructions, 23, 47-58.

Malvern L.E. (1969). "Introduction to the mecanics of a continuous medium", Englewood Cliffs, NJ: Prentice-Hall.

NP EN 206-1:2007, "Concrete – Part 1: Specification, performance, production and conformity", Norma Portuguesa, Instituto Português da Qualidade, Portugal, 2007.

ANNEX C

ROBUSTFIRE REPORT

Multi-level modelling strategy and verification

Authors:

Cheng Fang

Bassam Izzuddin

Ahmed Elghazouli

David Nethercot

Contents

I   Multi-level model

A multi-level modelling approach is presented for assessing the robustness of multi-storey buildings subject to localised fire. This modified approach is inspired by Izzuddin *et al.* (2008) for sudden column loss, where the ductility-centred method can be easily applied at various levels of structural idealisation, as illustrated in Figure 1. At the highest model level, the affected bay of the multi-storey building with appropriate boundary conditions is considered, as shown in Figure 1(a). Provided that the surrounding columns can resist the redistributed load, only the floors above the lost column need to be considered and the model is reduced to that shown in Figure 1(b). If the affected floors have identical structural geometry and gravity loading, a further reduced model consisting of an individual floor system may be considered, as illustrated in Figure 1(c). Finally, ignoring 2D effects (e.g. membrane action) of the floor slab, the model of Figure 1(c) can be reduced to a grillage model with each individual steel/composite beam resisting appropriate proportions of the gravity load, as shown in Figure 1(d). Since previous studies indicate that grillage models may underestimate the progressive collapse resistance of a structure due to the neglect of 2D slab effects, this section only introduces the application of the ductility-centred method on models employing 2D slab elements.
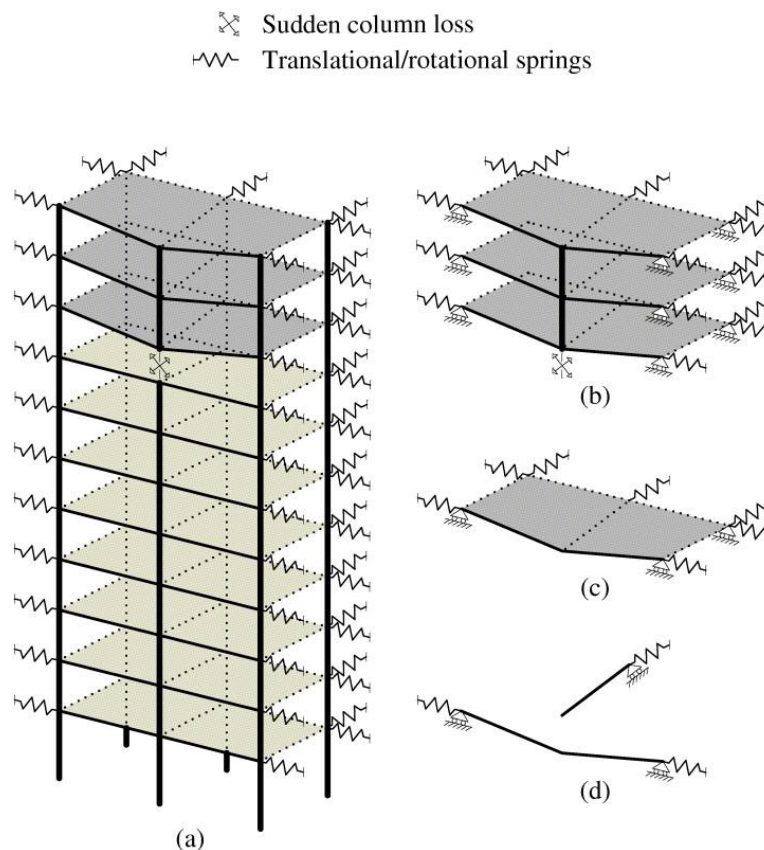

Fig. 1 Sub-structural model levels for progressive collapse assessment (Izzuddin *et al.*, 2008)

Based on the above idea, three modelling levels (A, B and C) can be generally employed for the current project, as shown in Figure 2. At level A, consideration is given to a whole system of the influenced sub-structure with appropriate boundary conditions representing the surrounding cool structures. Provided that the upper ambient floor systems have similar structure type and applied loading, the assessment model can be simplified to level B, where a reduced model consisting of the fire affected floor-column system and the upper ambient floor system are considered. At this level, the two systems (i.e. fire and ambient) are investigated separately. The derived characteristics of the ambient floors can be incorporated into a nonlinear 'spring' applied at the top of the fire-affected floor system. Then emphasis is given to the behaviour of the fire affected floor system with the added spring. Finally, at level C, 2D effects of the floor slab are ignored, and grillage models with composite beams are considered instead. The effective width of the slab flange can be obtained through Eurocode 4 (2004) considering shear lag, and the ribs can be ignored in the slab flange along the perpendicular direction.
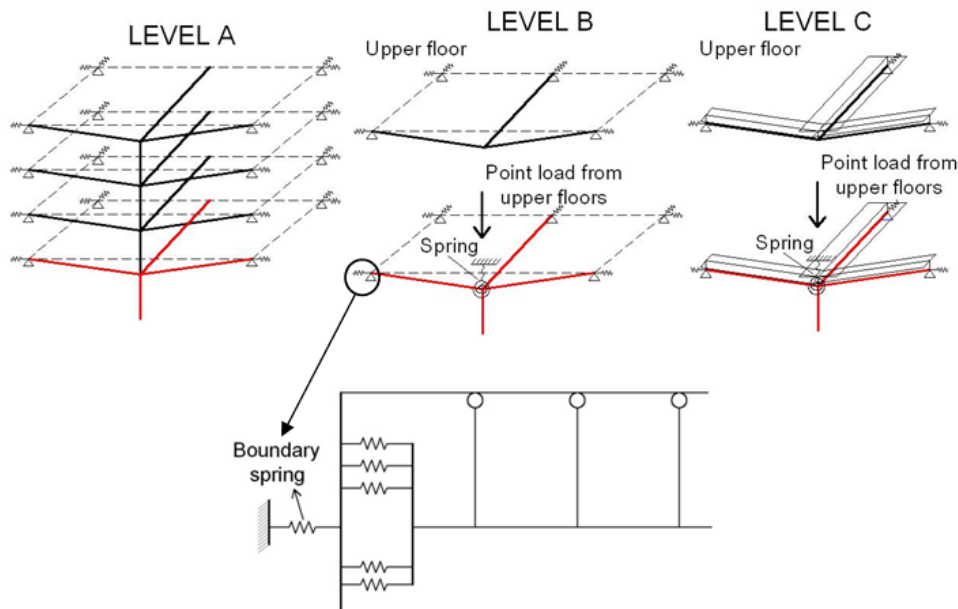

Fig. 2 Illustrative descriptions of three model levels

To obtain the response of the spring representing the upper ambient floors, a 5kN/m^2 UDL and an upward point load (exerted at the position of internal column) are initially applied to the ambient floor model. The upward point load is used to represent the supporting internal column, such that the initial floor deflection at the column location is zero. Subsequently, an increasing downward point load is exerted at the same position until one of the joints exceeds its ductility supply. Considering that a fire affected column will be subjected to thermal expansion, the evaluation of the upward stiffness of the ambient floor is also necessary. The rotational stiffness of the spring can be calculated as $4E_cI_c/L_c$, where E_c, I_c, and L_c are respectively the Young's modulus, the second moment of area, and the length of the column immediately above. For both model levels B and C, the initial load from upper ambient floors is

represented by a point load applied on top of the fire affected floor with a value taken as $0.25P_{gravity}$ (Vlassis *et al.*, 2008; Izzuddin, *et al.*, 2008), where $P_{gravity}$ is the overall gravity loading applied on the upper ambient double-span floors.

II Verification of model reduction

In order to verify the accuracy of the proposed model reduction procedure, a four-storey steel-framed composite structure is established in ADAPTIC (Izzuddin, 1991), as shown in Figure 3(a). Joint details are ignored in the model, and beams and columns are assumed to be rigidly connected. All the boundary springs are considered as fully restrained. It is assumed that the internal column at the ground floor experiences a uniform increase in temperature, and this temperature reduces linearly from the column top to room temperature 3m away from the column within the connected steel beams. The slab is considered as fully protected and remains under ambient conditions throughout the heating procedure. This model is then reduced to a level C model comprising the fire floor system and an additional spring, as shown in Figure 3(b). The downward and upward stiffness of one ambient floor is given in Figure 4. In ADAPTIC, the spring is modelled using an element that is capable of simulating the force-displacement relationships with multi-linear approximations. The loads exerted onto the reduced model include a 5kN/m^2 UDL, a point load from the upper three ambient floors and the subsequent thermal load.
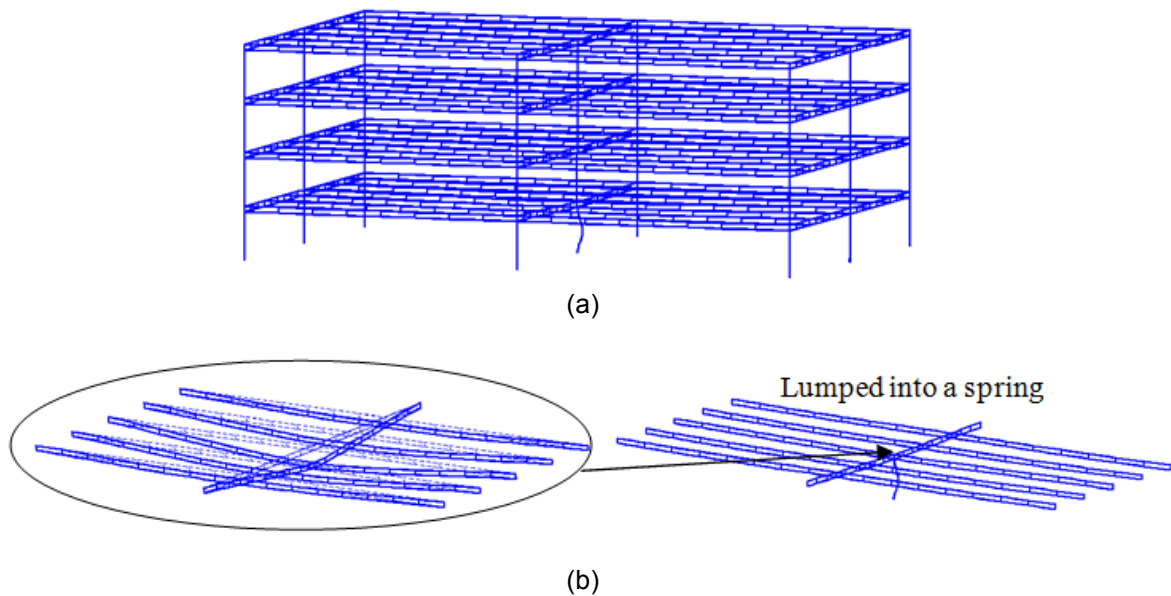

(a)

(b)

Fig. 3 Deflection shape of ADAPTIC model with internal column at 1000ºC: (a) 4-storey model, (b) reduced system model
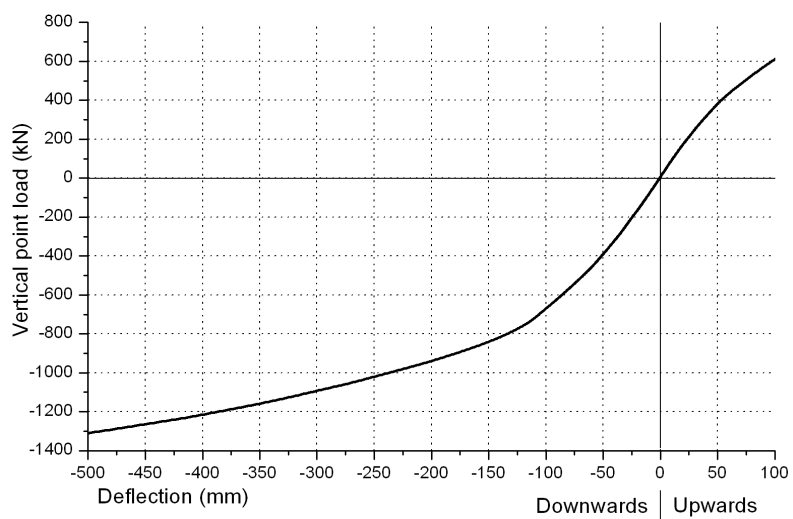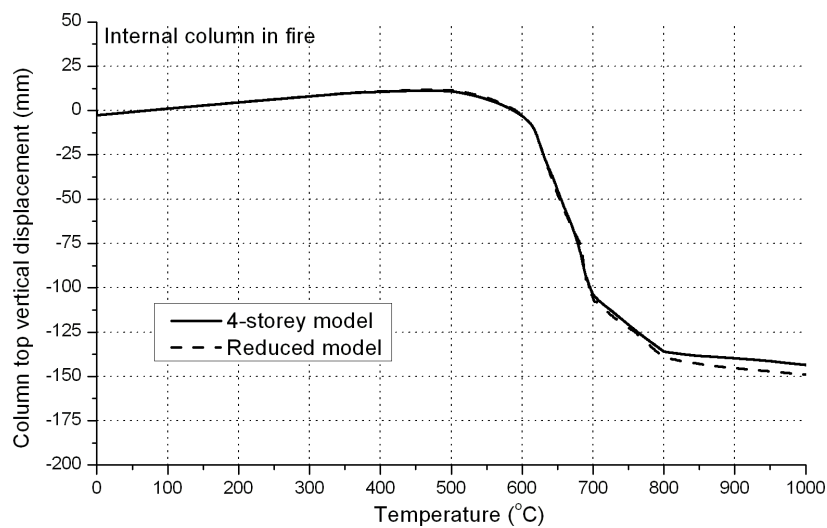
Fig. 4 Response of one ambient floor

Fig. 5 Variation of vertical displacement at column top
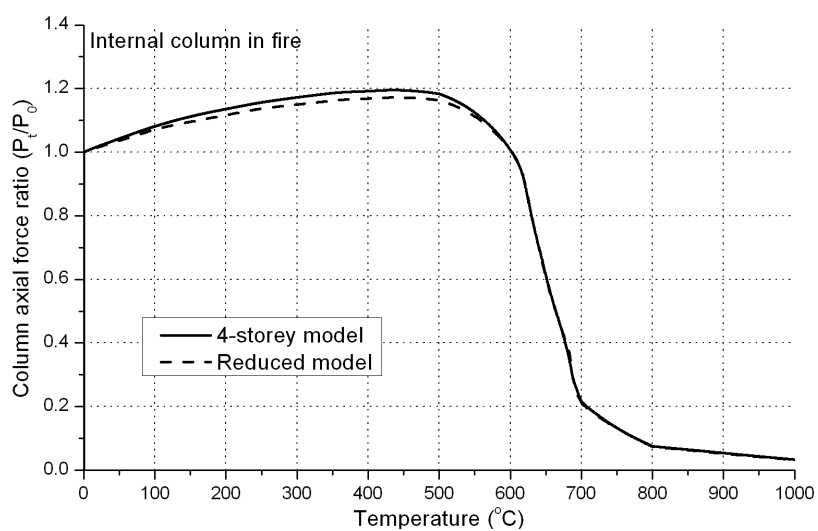

Fig. 6 Variation of column axial force

Figure 5 presents the vertical displacement at the column top for the 4-storey model as well as the reduced system model, while Figure 6 provides the column axial force ratio P_t/P_0 from the two models, where P_t is the axial force of the heated column, and P_0 is the initial column axial force under the ambient condition. The peak column axial force ratio P_t/P_0, the maximum floor deflection, and the critical temperature of the two levels of the models are listed and compared in Table 1, where the critical temperature is defined at the instant when the column internal axial force returns back to its initial value under ambient temperature. It is found that the responses of the two models are very close, which verifies that a reduced system model is capable of capturing the behaviour of the structures subject to localised fire with sufficient accuracy compared with more complex multi-storey models, provided that the response of upper ambient floors is accurately modelled.

Table 1 Comparison of data between two models with internal column under fire

Structural response	Full 4-storey model	Reduced system model	Discrepancy
Maximum column axial force ratio P_t/P_0	1.195	1.172	1.92%
Vertical deflection at 1000°C(mm)	143.5	148.9	3.76%
Critical temperature (°C)	601.8	602.5	0.12%

III Conclusions

A multi-level modelling approach, which simplifies a complex multi-storey structural model into a reduced single-storey system model, has been developed for assessing the robustness of multi-storey buildings subject to localised fire. The new apporach draws on the multi-level modelling idea proposed by Izzuddin *et al.* (2008) for sudden column loss. This report verifies the rationale behind the proposed model reduction approach. Provided that the response of upper ambient floors is appropriately predicted, a reduced system model possesses sufficient accuracy compared with more complex multi-storey models. Therefore, efficient reduced system models can be confidently used for further assessments of structural robustness of car parks subject to localised fires.

IV References

EN 1994-1-1:2004. "Eurocode 4: Design of composite steel and concrete structures – Part 1-1: General rules and rules for buildings". European committee for standardization, December 2004.

Izzuddin, B.A. (1991) Nonlinear Dynamic Analysis of Framed Structures. PhD Thesis. Department of Civil Engineering, Imperial College, University of London, London, UK.

Izzuddin B.A., Vlassis A.G., Elghazouli A.Y. and Nethercot D.A. Progressive Collapse of Multi-Storey Buildings due to Sudden Column Loss – Part I: Simplified Assessment Framework. Engineering Structures, 2008, 30, No.5, pp. 1308-1318.

Vlassis A.G., Izzuddin B.A., Elghazouli A.Y. and Nethercot D.A. Progressive Collapse of Multi-Storey Buildings due to Sudden Column Loss – Part II: Application. Engineering Structures, 2008, 30, No.5, pp. 1424-1438.